Journal of Medicinal Chemistry

Article

Design, synthesis and in vitro and in vivo evaluation of an 18F-labeled sphingosine 1-phosphate receptor 1 (S1P1) PET tracer

Adam J Rosenberg, Hui Liu, Hongjun Jin, Xuyi Yue, Sean Riley, Steven J Brown, and Zhude Tu

J. Med. Chem., **Just Accepted Manuscript** • DOI: 10.1021/acs.jmedchem.6b00390 • Publication Date (Web): 09 Jun 2016

Just Accepted

ACS Publications

Journal of Medicinal Chemistry is published by the American Chemical Society. 1155 Sixteenth Street N.W., Washington, DC 20036

Design, synthesis and *in vitro* and *in vivo* evaluation of an ^{18}F-labeled sphingosine 1-phosphate receptor 1 ($S1P_1$) PET tracer

Adam J. Rosenberg[a], Hui Liu[a], Hongjun Jin[a], Xuyi Yue[a], Sean Riley[b], Steven J. Brown[b], and Zhude Tu[a]*

[a] Department of Radiology, Washington University School of Medicine, 510 South Kingshighway Boulevard, St. Louis, Missouri 63110

[b] The Scripps Research Institute Molecular Screening Center, 10550 N. Torrey Pines Rd., La Jolla, CA 92037

ABSTRACT: Sphingosine 1-phosphate receptor 1 ($S1P_1$) plays a pivotal signaling role in inflammatory response; because $S1P_1$ modulation has been identified as a therapeutic target for various diseases, a PET tracer for $S1P_1$ would be a useful tool. Fourteen fluorine-containing analogues of S1P ligands were synthesized and their *in vitro* binding affinities measured; four had high affinity and selectivity for $S1P_1$ ($S1P_1$ IC_{50} < 10 nM, > 100-fold selectivity for $S1P_1$ over $S1P_2$ and $S1P_3$). The most potent ligand, **28c** (IC_{50} = 2.63 nM for $S1P_1$) was ^{18}F-labeled and evaluated in a mouse model of LPS-induced acute liver injury to determine its $S1P_1$-binding specificity. The results from biodistribution, autoradiography, and microPET imaging showed higher [^{18}F]**28c** accumulation in the liver of LPS-treated mice than controls. Increased expression of $S1P_1$ in the LPS model was confirmed by IHC. These data suggest that [^{18}F]**28c** is a $S1P_1$- PET tracer with high potential for imaging $S1P_1$ *in vivo*.

1. INTRODUCTION

Sphingosine 1-phosphate (S1P, Fig. 1) receptors are a class of G-protein-coupled receptors (GPCRs) with five distinct subtypes, denoted as $S1P_{1\text{-}5}$.[1, 2] These receptors are regulated by S1P and have important regulatory functions in both normal biological processes and in disease; particularly in pathological processes involving the immune system, the CNS, and the cardiovascular system. Because the S1P/S1P-receptor pathway is especially important in cancer and autoimmune disorders including multiple sclerosis (MS), tremendous development efforts have focused on therapeutically targeted S1P receptor ligands. These efforts discovered a promising compounds, 2-amino-2-[2-(4-octyl-phenyl)-ethyl]-propane-1,3-diol **1** (FTY720, Fingolimod, Fig. 1), that was approved by the US Food and Drug Administration (FDA) for treatment of relapse remitting multiple sclerosis in 2010. Compound **1** is phosphorylated *in vivo* by sphingosine kinase 2, this stereospecific process generates the biologically active metabolite (*S*)-FTY720-Phosphate (**(*S*)-1-P**, Fig. 1), a potent S1P receptor agonist.[3-5] **(*S*)-1-P** is a nonselective S1P receptor ligand, which binds to each of the S1P receptor subtypes except $S1P_2$. Since its primary mechanism of action in MS is believed to be through $S1P_1$,[4] recent development has focused on ligands having high potency and selectivity for $S1P_1$ with suitable pharmacological properties for therapeutic applications. Although rodent studies using S1P receptor ligands suggested that adverse cardiovascular effects were the result of $S1P_3$ agonism,[6, 7] the Phase I study of a $S1P_1$ selective therapeutic reported bradycardia associated with the first dose administered to human subjects.[8] Because activity at $S1P_3$ has clear effects on the vascular system and does not appear to contribute to therapeutic efficacy of these ligands in the immune system,[9] our efforts have focused on identifying subtype-selective ligands. $S1P_1$ ligands are also being evaluated in cancer,[10, 11] rheumatoid arthritis,[12] ulcerative colitis,[13, 14] as well as liver and lung injury among other therapeutic uses.[15-18]

Positron emission tomography (PET) is a widely utilized imaging modality which can be used to non-invasively quantify molecular targets *in vivo*. PET is used in drug discovery to assess receptor occupancy, downstream functional changes, and impact on disease pathophysiology.[19] A $S1P_1$ specific PET tracer could greatly assist the evaluation of new therapeutics by measuring the relationship between drug exposure (dose administered or plasma concentration) and receptor occupancy, thus enabling accelerated dose selection during early clinical trials.[20-22] A successful PET ligand should have a binding affinity < 10 nM and must be specific to the target versus neighboring non-target tissues to allow for quantification of the regions of interests during the timeframe of clinical studies (0-2 hours).[23, 24]

To date, no S1P receptor imaging agent suitable for clinical studies has been reported, although since 2011, several groups have reported their efforts to develop a $S1P_1$ receptor tracer.[25-27] The iodinated analogue, 2-amino-2-[2-(2-iodo-4-

octylphenyl)ethyl]-1,3-propandiol **2** (BZM055, Fig. 2), was ^{123}I-labeled for single photon emission computed tomography (SPECT) studies, and could be ^{124}I-labeled for PET imaging.[25] Although compound **2** showed pharmacokinetic trends similar to compound **1**, its lower rate of phosphorylation (required for receptor binding) compared to compound **1** limits its effectiveness as an imaging agent. The long half-lives of either iodine-123 ($t_{1/2}$ = 13.2 h) or iodine-124 ($t_{1/2}$ = 4.2 days) would enable study of both the distribution kinetics of the parent ligand and its elimination kinetics. Haufe and co-workers separately reported ^{18}F-labeled PET imaging agents based on the only known $S1P_1$ antagonist, [(3*R*)-amino-4-[(3-hexylphenyl)amino]-4-oxobutyl]-phosphonic acid, mono(trifluoroacetate) (W146),[26] and based on compound **1**.[27] (Fig. 2) The ^{18}F-labeled W146 analog (*R*)-1-[[3-(6-fluorohexyl)phenyl]amino-4-oxobutyl]phosphonic acid, ([^{18}F]**3)** was shown to bind with $S1P_1$, and unlike **1** does not require a preliminary phosphorylation step for binding potency. However, despite its *in vitro* stability in mouse serum, PET imaging of [^{18}F]**3** in wild-type mice showed rapid total body clearance as well as bone uptake, which is a measure of *in vivo* defluorination. Their recent report describes the more favorable evaluation of ^{18}F-labeled **2** analogues, with either an 8-carbon (2-amino-2-[4-(8-fluorooctyl)phenethyl]propane-1,3-diol, [^{18}F]**4a**) or a 6-carbon (2-amino-2-[4-(6-fluorohexyl)phenethyl]propane-1,3-diol, [^{18}F]**4b**) aliphatic tail (Fig. 2). The ligand with the shorter tail, [^{18}F]**4b**, showed reduced *in vitro* activity, but both tracers demonstrated uptake in S1P target organs of wild-type mice with no evidence of *in vivo* defluorination. Unlike [^{18}F]**3**, the **1** analogues require phosphorylation before binding to S1P receptors. While potentially useful tools, at this time it is unclear how rapidly and to what extent the ligands undergo phosphorylation during the typical time frame for PET imaging (1-2 h post-injection).

We have also used the wealth of knowledge in this field to investigate PET radiotracers for S1P receptors using rodent models of human disease.[28-30] Our group previously reported the radiosynthesis of the ^{11}C-labeled $S1P_1$ selective ligand 3-((2-fluoro-4-(5-(2'-methyl-2-(trifluoromethyl)-[1,1'-biphenyl]-4-yl)-1,2,4-oxadiazol-3-yl)benzyl)-(methyl)amino)-propanoic acid **5** ([^{11}C]TZ3321, Fig. 2) and demonstrated the feasibility of PET imaging $S1P_1$ as a measure of inflammatory response in both the femoral artery wire-injury mouse model of restenosis[29] and in the experimental autoimmune encephalomyelitis (EAE) rat model of multiple sclerosis (MS).[30] Here, we present the synthesis and screening of fluorine-containing ligands based on reported compounds with either a benzoxazole core,[31] or an oxadiazole core.[32, 33] Compound **28c** was identified as a potent and selective ligand for $S1P_1$ over $S1P_2$ or $S1P_3$ in our competitive binding assay, [34] so was ^{18}F-labeled for biological evaluation in the mouse model of LPS-induced liver injury.

2. RESULTS AND DISCUSSION

The synthetic strategy is discussed in detail below, but the two lead compounds used for development of an ^{18}F-labeled tracer were selected due to published data indicating that they are not prodrugs which require *in vivo* phosphorylation, and due to their favorable biological behavior.[31, 32] Our screening focused on $S1P_1$ selective ligands because the efficacy of **2** in MS is attributed to its high binding potency toward to $S1P_1$.[6, 35] As shown in Table 2, **28c** has a high potency (IC_{50} = 2.63 ± 0.27 nM) and selectivity for $S1P_1$ over $S1P_2$ or $S1P_3$ (IC_{50} > 1000 nM). The synthesis of [^{18}F]**28c** was accomplished. the mouse model of LPS-induced acute liver injury was used for the *in vivo* evaluation of [^{18}F]**28c**. Biodistribution studies carried out with both [^{18}F]**28c** and the liver imaging agent [^{99m}Tc]-*N*-(3-bromo-2,4,6-trimethyacetanilide) iminodiacetic acid ([^{99m}Tc]mebrofenin) in LPS and sham mice.[36] The absence of a significant difference between the two tracers in this model 60 min post-injection suggested that the higher liver uptake of [^{18}F]**28c** in LPS-treated mice compared to control mice was not caused by reduced hepatobiliary clearance in the liver injury model. MicroPET imaging in LPS and sham treated mice also showed increased retention of [^{18}F]**28c** in the injured liver which correlated with increased $S1P_1$ expression observed in IHC studies, while no difference in liver uptake of [^{15}O]water was seen between LPS-treated and sham mice,[37, 38] suggesting the higher injured liver accumulation of [^{18}F]**28c** is not due to a change in blood flow in injured liver. These data indicate liver uptake of [^{18}F]**28c** correlates well with the expression of $S1P_1$ in mouse liver.

2.1 Chemistry

Ligands with a benzoxazole core were prepared as shown in Schemes 1 & 2. The starting halogenated trifluoromethylbenzoic acids were functionalized by either palladium catalyzed Suzuki coupling with the desired aryl boronic acid to provide the biaryl moieties, or by nucleophilic aromatic substitution with the desired alcohol to give the ethereal products. The appendant carboxylic acid was transformed to the corresponding acid chloride with oxalyl chloride and catalytic DMF, which was then reacted with a functionalized 2-hydroxyaniline under Schotten–Baumann conditions to give amides **10**. These amides were subsequently heated under acidic conditions to cyclize and provide the benzoxazole cores. The installation of the polar head groups was accomplished by a variety of methods. *β*-Amino acids **15a** and **15b**, were prepared by reduction of a methyl ester to an alcohol, and functional group transformation to a chloride, and subsequently to the azetidine ester, which was unmasked to provide **15**. Acid **16** was prepared by a Suzuki coupling with a thiophene boronic acid. Palladium-catalyzed amination with methyl piperidine-4-carboxylate gave the protected products, which were subsequently saponified to give acids **18**.

Ligands with an oxadiazole core were synthesized according to Scheme 3. The required carboxylic acids were prepared as above, or from methyl 4-hydroxybenzoate (**22**) by alkylation and saponification. The desired carboxylic acid was reacted

with *N'*-hydroxy-4-(hydroxymethyl)benzimidamide (**25**) under standard peptide coupling conditions, and subsequently thermally cyclized to give the oxadiazole cores. *O*-(Benzotriazol-1-yl)-*N,N,N',N'*-tetramethyluronium tetrafluoroborate (TBTU) was also used as a coupling agent, followed by thermal cyclization.[39] The appendant benzyl alcohol was oxidized under Swern conditions to give aldehydes **27**. The β-amino acid head group was affixed by reductive amination with the desired amine to provide the targeted ligands **28a-f**. The lipophilicity of a radiotracer, expressed as logP, impacts nonspecific binding and its ability to cross the BBB, which is a key physical constraint for targets in CNS and intracellular targets including enzymes.[40] The calculated lipophilicity at a pH of 7.4 of the new compounds is reported as cLogD values in Tables 1-2. The oxadiazole **28c** had cLogD of 2.32 which is within the desired range for CNS tracers and, as discussed below, a favorable *in vitro* binding profile, thus we elected to pursue its development as a radiotracer and synthesized precursors for radiolabeling. Precursor **32** for radiolabeling [^{18}F]2-fluoroethyltosylate was prepared from phenol **29,** as shown in Scheme 4, using a synthetic route similar to that used for the oxadiazole analogues. Formation of the oxadiazole proceeded as expected, however the oxidation step required different conditions due to the presence of the unprotected phenol. Oxidation with manganese (IV) oxide provided smooth conversion to desired aldehyde **31**. Reductive amination under buffered conditions afforded **32**. Precursor **34** for direct labeling was also prepared as shown in Scheme 5. Starting with aldehyde **31**, the free phenol was alkylated with ethylene ditosylate to provide compound **33**, which was subjected to reductive amination to yield **34**. The reductive amination conditions were modified to utilize sodium triacetoxyborohydride, because harsher reducing agents tended to reduce the alkyl tosylate.

2.2 *In Vitro* Binding Assays

Competitive inhibition of the binding of radiolabeled [^{32}P]S1P to the new analogues was measured to determine the affinity of the ligands for $S1P_1$, $S1P_2$, and $S1P_3$.[34] The results are reported in Tables 1 and 2. The benzoxazole series of ligands displayed nanomolar activity in the functional assay (EC_{50}), however the ligands displayed lower binding affinity for $S1P_1$ in the competitive binding assay (IC_{50}). Although the reason for this discrepancy in the assay results is not clear, similar results have observed with other S1P receptor ligands.[41] Additionally while functional assays can be extremely useful in the preliminary stages of imaging agent development, the binding affinity of a ligand cannot be determined without a competitive binding assay.[42] While none of the ligands in this series had sufficient binding affinity (IC_{50} < 10 nM) to be pursued as a PET tracer, structure-activity relationships (SAR) became apparent. The residues and shape of the $S1P_1$ binding pocket have been well documented with a published crystal structure.[43] The binding pocket consists of two major components, a charged head portion and a lipophilic tail area. The strong recognition for ligand binding is thought

to be derived from interactions between the positively charged Arg^{120} and the phosphate in S1P, and interactions between the negatively charged Glu^{121} and the ammonium in S1P. The lipophilic part of the binding pocket appears to be quite tolerant of a variety of functional groups, with the noted exception of the *ortho*-substituted fluoroethyl ether **18b** (IC_{50} = 894 ± 367 nM).

The oxadiazole ligand series showed much more promise than the benzoxazole series, as seen in Table 2. We explored the effects of modifying the lipophilic side-chain of **28a** (IC_{50} = 8.53 ± 3.14 nM). Addition of a fluorine (**28b**, IC_{50} = 9.94 ± 1.03 nM) had no significant change on the binding affinity, while an ortho-trifluoromethyl group noticeably improved the affinity to 2.63 ± 0.27 nM (**28c**). Next we turned to the polar head-group. While some $S1P_1$ ligands without a polar head-group have a high degree of potency, we elected to maintain this property in our explorations. Changing the azetidine ring of **28c** to a piperidine (**28d**) gave a 20-fold decrease in binding affinity to 45.4 ± 2.7 nM. Bioisosteric substitution of the acid to a tetrazole resulted significant loss of activity of over 100-fold to 509 ± 167 nM (**28e**), while shortening the two-carbon tail to a methyl group adversely impacted the binding affinity giving an IC_{50} > 100 nM (**28f**). Finally, the benzyl alcohol **26c** was synthesized to determine how critical the amino acid head group was, surprisingly this head group was not required as **26c** was quite potent with an IC_{50} of 6.67 ± 0.70 nM. All compounds with a binding affinity under 50 nM were screened for selectivity versus $S1P_2$ and $S1P_3$; no tested compounds showed detectable binding with $S1P_2$ or $S1P_3$. **28c** had a high potency for $S1P_1$ (IC_{50} = 2.63 ± 0.27 nM) with no measurable potency for $S1P_2$ (IC_{50} >1000 nM) or $S1P_3$ (IC_{50} >1000 nM) with a cLogD of 2.32, thus we elected to pursue **28c** as our lead compound for ^{18}F-labeling.

2.3 Radiochemistry

The radiosynthesis of **28c** was initially attempted using the versatile indirect approach of labeling with [^{18}F]2-fluoroethyltosylate. The precursor **32** was prepared as shown in Scheme 4. Unfortunately attempts to label **32** indirectly resulted only in extremely low yields under a variety of conditions (< 5% radiochemical yield for the alkylation step), likely due to the low nucleophilicity of the electron-deficient phenol. Due to this concern, as well as a desire to avoid a three-step, two-pot radiosynthesis, we subsequently pursued a direct labeling approach starting with the tosylate precursor (**34**) as shown in Scheme 6.

The tosylate precursor (**34**) was reacted with Kryptofix 222 (K_{222}), and [^{18}F]KF in acetonitrile for 15 min at 110 °C to install the fluoroethyl tail. The carboxylic acid head group was unmasked by saponification with sodium hydroxide. The resulting crude product was purified by high performance liquid chromatography (HPLC) to give [^{18}F]**28c** in 25.7 ± 4.6%

(n = 10, decay corrected to start of synthesis), with >98% chemical and radiochemical purity, and a high specific activity (1.43 ± 0.12 Ci/μmol).

2.4 Biological Studies

2.4.1 Biodistribution in normal rats

To investigate the tissue distribution of [^{18}F]**28c** in living subjects, a biodistribution study was performed in adult male Sprague-Dawley (SD) rats. As shown in Table 3, the results showed significant uptake and retention in the liver, without evidence of *in vivo* defluorination (no increased accumulation in bone was observed from 5 to 120 min post-injection). Relatively high uptake was observed for the heart, lungs, pancreas, and spleen; all organs known to have high $S1P_1$ expression. The surprisingly low brain uptake of [^{18}F]**28c** as shown in Table 3, may potential limit its utility for CNS applications.

2.4.2 *In vitro* autoradiography and IHC in LPS-treated mice

We utilized the mouse model of LPS-induced liver injury and inflammation, in which inflammation caused by LPS is known to cause increased liver expression of $S1P_1$ after ~ 24 h to evaluate [^{18}F]**28c** in tissue from an animal model of inflammatory disease.[44, 45] *In vitro* autoradiographic data showed increased uptake of [^{18}F]**28c** in the liver of LPS-treated mice, compared with the sham liver shown in Fig. 3A. The specificity of [^{18}F]**28c** for $S1P_1$ was demonstrated by incubation of adjacent mouse liver slices with the tracer in presence of either the native ligand (S1P) or the $S1P_1$ selective compound, SEW2871.[46] The upregulation of $S1P_1$ in the liver at the 24 h time point following LPS treatment was further confirmed by IHC staining shown in Fig. 3B. These blocking studies in conjunction with the IHC results suggest that the binding of [^{18}F]**28c** in the liver of LPS-treated mice is the result of specific binding to the receptor and is increased when $S1P_1$ expression is increased.

2.4.3 MicroPET imaging of LPS-treated mice with [^{18}F]28c and [^{15}O]water

Subsequent microPET imaging in the LPS model of liver inflammation also clearly showed increased accumulation of [^{18}F]**28c** in the liver of LPS-treated mice compared to sham controls (Fig. 4A). Time-activity curves (TAC) confirmed higher tracer uptake in the liver of LPS pre-treated mice compared with the sham controls (Fig. 4B). Quantification of the liver region of interest (ROI) in the microPET scan from 100-120 min shows a 61% increase ($P < 0.001$, $n = 4$) (Fig. 4C). These results were confirmed by euthanasia of the mice post PET for an acute biodistribution study. The liver uptake of [^{18}F]**28c** in the LPS treated mouse at 2 h was 1.95-fold higher than that in the sham mice (12.5 vs. 24.4 % ID/gram, $P < 0.001$, $n = 4$).To further demonstrate that the increased uptake of [^{18}F]**28c** in the liver was not attributed to changes in

blood flow in the LPS-induced model of liver injury, additional microPET studies were performed with an injection of [^{15}O]water 30 min prior to injection of [^{18}F]**28c**. [^{15}O]Water is a widely radiotracer for assessing blood flow.[47, 48] As shown in Fig. 4D, the liver TAC for [^{15}O]water in LPS treated mice showed no significant change compared to that in the sham mice. This suggested the increase *in vivo* uptake of [^{18}F]**28c** in the liver of LPS-treated mice is the result of increased $S1P_1$ expression and not increased blood flow.

2.4.3 Biodistribution of [^{18}F]28c and [^{99m}Tc]Mebrofenin in LPS-treated mice

To confirm that the uptake of [^{18}F]**28c** was associated with $S1P_1$ expression, we utilized a mouse model of LPS-induced liver injury and inflammation, in which inflammation caused by LPS is known to cause increased liver expression of $S1P_1$ after ~ 24 h.[44, 45] Biodistribution studies comparing of [^{18}F]**28c** uptake in saline-treated sham controls vs. the LPS-treated mouse model demonstrated a large increase in liver uptake (Fig. 5). In order to demonstrate that tracer retention in the liver was not due to impaired hepatobiliary clearance in the liver injury model, an additional study was carried out with this model using a liver imaging agent. [^{99m}Tc]Mebrofenin is used to detect if the hepatobiliary transport is impaired. Increased liver uptake of [^{99m}Tc]mebrofenin indicates the potential for non-specific retention of drugs (in this case, [^{18}F]**28c**) in the liver due to impaired clearance, rather than uptake specific to the pathological increase in $S1P_1$ at the molecular level.[36, 49, 50 32, 33] We hypothesized that increased liver uptake of [^{99m}Tc]mebrofenin in LPS-treated mice versus the sham control mice at 60 min would suggest that increased uptake of the $S1P_1$ tracer resulted from severely damaged liver, however if the liver uptake of [^{99m}Tc]mebrofenin in LPS-treated mice versus the sham mice was similar at 60 min (as we observed), the increase should reflect an increase in $S1P_1$ rather than impaired clearance.[36, 49] To confirm that this increase in uptake of [^{18}F]**28c** resulted from the increase expression of $S1P_1$ receptor response to liver injury, the biodistribution study of [^{99m}Tc]mebrofenin was performed in the LPS-induced liver injury models. Although increased [^{99m}Tc]mebrofenin was observed in the liver of LPS-treated mice at 30 min p.i. compared with sham mice, at 60 min p.i. there was no significant difference between the sham and LPS study groups. The uptake of [^{18}F]**28c** showed a significant increase in the LPS-treated mice compared to the sham control mice at both 30 min and 60 min (Fig. 5). The biodistribution data demonstrated that the increased hepatobiliary uptake of [^{18}F]**28c** in LPS-treated mice is mainly caused by the upregulation of $S1P_1$ expression in the liver.

3. CONCLUSIONS

We synthesized fourteen fluorine-containing analogues based on two lead pharmacophores and determined their affinity for $S1P_1$. Potent compounds (IC_{50} < 50 nM for $S1P_1$) were subsequently screened for their $S1P_2$ and $S1P_3$ binding

affinities. Seven compounds were found to have IC_{50} values < 100 nM while three were very potent with $S1P_1$ IC_{50} values < 10 nM. We explored the SAR studies on the oxadiazole containing pharmacophore by optimizing the lipophilic tail binding portion of the binding pocket. The oxadiazole **28c** had a high potency (2.63 nM for $S1P_1$) and selectivity (>100-fold for $S1P_1$ versus $S1P_{2/3}$), and was successfully radiolabeled in high yield and high specific activity. Biodistribution in normal rats showed no evidence of defluorination, so the a mouse model of liver inflammation was used for subsequent biological evaluation of [^{18}F]**28c** as a PET tracer for imaging $S1P_1$. *In vitro* autoradiography and microPET imaging studies showed increased increased binding *in vitro* and *in vivo* retention of [^{18}F]**28c** in the liver of LPS-treated vs. control mice. IHC staining studies confirmed that $S1P_1$ expression was increased in the liver of LPS-treated mice. Additional microPET imaging showed no difference in liver uptake of [^{15}O]water between LPS-treated and control mice,[37, 38] further supporting the hypothesis that the higher uptake and retention of [^{18}F]**28c** in the liver of LPS-treated mice was a reflection of increased $S1P_1$ due to inflammation and not due to a change in blood flow. Parallel acute biodistribution studies in the LPS model were carried out with both [^{18}F]**28c** and the liver imaging agent [^{99m}Tc]mebrofenin.[36] The absence of a significant difference in liver uptake of [^{99m}Tc]mebrofenin in LPS-treated vs. control liver uptake 60 min post-injection suggested that the increased liver uptake of [^{18}F]**28c** in observed in the PET studies of LPS-treated mice was not the result of reduced hepatobiliary clearance due to liver injury. Together these data indicate uptake of [^{18}F]**28c** reflects the expression of $S1P_1$ and suggest that [^{18}F]**28c** is a $S1P_1$ specific radiotracer with potential for use in quantifying $S1P_1$ receptor expression in response to inflammation.

4. EXPERIMENTAL SECTION

4.1 Chemistry Materials and Methods

Unless otherwise indicated, all reactions were conducted in oven-dried (140 °C) glassware. Stainless steel syringes or cannulae that had been oven-dried (140 °C) and cooled under a nitrogen atmosphere or in a desiccator were used to transfer air- and moisture-sensitive liquids. Yields refer to chromatographically and spectroscopically (^{1}H NMR) homogeneous materials, unless otherwise stated. Reactions were monitored by thin-layer chromatography (TLC) carried out on precoated glass plates of silica gel (0.25 mm) 60 F_{254} from EMD Chemicals Inc. Visualization was accomplished with ultraviolet light (UV 254 nm), or by shaking the plate in a sealed jar containing silica gel and Iodine. Alternatively, plates were treated with one of the following solutions (this was accomplished by holding the edge of the TLC plate with forceps or tweezers and immersing the plate into a wide-mouth jar containing the desired staining solution) and carefully heating with a hot-air gun (450 °C) for approximately 1-2 min (NOTE: excess stain was removed by resting the TLC on a

paper towel prior to heating): 10% phosphomolybdic acid in ethanol, 1% potassium permanganate/7% potassium carbonate/0.5% sodium hydroxide aqueous solution, and/or anisaldehyde in ethanol with 10% sulfuric acid. Flash column chromatography was performed using Silia Flash® P60 silica gel (40-63 μm) from Silicycle. All work-up and purification procedures were carried out with reagent grade solvents in air.

^{1}H NMR spectra were recorded on Varian 400 MHz instrument. Chemical shifts are reported in parts per million (ppm) and are calibrated using residual undeuterated solvent as an internal reference ($CDCl_3$: δ 7.26 ppm; MeOD-d4: δ 3.31 ppm; DMSO-d6: δ 2.50 ppm). Data are reported as follows: chemical shift, multiplicity, coupling constants (Hz), and integration. The following abbreviations or combinations thereof were used to explain the multiplicities: s = singlet, d = doublet, t = triplet, q = quartet, pent = pentet, sext = sextet, sept = septet, m = multiplet, at = apparent triplet, aq = apparent quartet, b = broad. ^{13}C NMR spectra were recorded on a Varian instrument (100 MHz) spectrometer with complete proton decoupling. Chemical shifts are reported in ppm and are calibrated using residual undeuterated solvent as an internal reference ($CDCl_3$: δ 77.16 ppm; MeOD-d4: 49.00 ppm; DMSO-d6: 39.52 ppm). Elemental compositions (C, H, N) are within ±0.4% of the calculated values, and were determined by Atlantic Microlab, Inc. Lipophilicity values as cLogD are reported as the calculated Log P value at pH = 7.4, and were obtained using ACD/I-Lab ver. 7.0 (Advanced Chemistry Development, Inc. Toronto, Ontario, Canada). All the final compounds for which the biologic activity was determined by analytical HPLC method with purity ≥ 95%.

4.1.1 Synthesis

General Procedure A: Suzuki Coupling. To an oven-dried round-bottom flask equipped with a stirbar was added $Pd(OAc)_2$ (2 mol %), 2-dicyclohexylphosphino-2',6'-dimethoxybiphenyl (SPhos, 5 mol %), commercially available 4-bromo-3-(trifluoromethyl)benzoic acid (**6**) (1 equiv), the boronic acid (1.1 equiv), and a fluoride base (3 equiv). 1,4-dioxane (0.37 M) and degassed H_2O (0.37 M) were added to the reaction mixture and the reaction was degassed by splurging with $N_{2(g)}$ for 10 min, at which time it was equipped with a condenser and placed in a pre-heated 110 °C oil-bath. The reaction mixture was stirred for the time indicated, cooled to room temperature (r.t.) and poured into a 1:1 mixture of ethyl acetate and 1N $HCl_{(aq)}$. The quenched reaction mixture was stirred for 20 min, and the layers were then separated. The aqueous layer was extracted with ethyl acetate (×2). The combined organic layers were dried over MgSO4, concentrated *in vacuo* and purified as specified.

General Experimental B: Amide Formation. To an oven-dried round-bottom flask equipped with a stirbar was added the carboxylic acid (1 equiv) followed by CH_2Cl_2 (0.1 M). Five drops of *N,N*-dimethylformamide was added via pipette

followed by a slow addition of oxalyl chloride (2.3 equiv) via syringe. The reaction was then stirred at r.t. for 2 h, at which time it was concentrated *in vacuo*. The crude acid chloride was then dissolved in toluene (0.15 M) and 10% $NaHCO_{3(aq)}$ (0.3 M) was added. The aniline **9a** or commercially available 2-amino-4-bromophenol (**9b**) (1 equiv) was added and the reaction was stirred overnight. Upon completion of the reaction, the resulting precipitate was filtered, and washed with H_2O, toluene, and hexanes to give the desired amide.

General Experimental C: Benzoxazole Formation. To a round-bottom flask equipped with a stirbar was added the amide (1 equiv), toluene (0.1 M), and *p*-toluenesulfonic acid (2.1 equiv) or pyridinium *p*-toluenesulfonate (2.1 equiv). The reaction was equipped with a reflux condenser and lowered into a pre-heated 130 °C oil-bath. The reaction mixture was stirred for the specified time, cooled to r.t., diluted with EtOAc, and washed with: sat. $NaHCO_{3(aq)}$ (×2), and brine. The organic layer was dried over $MgSO_4$ and concentrated *in vacuo* to give the desired benzoxazole.

General Procedure D: Buchwald-Hartwig Coupling. To an oven-dried flask (pressure-vessel or Schlenk tube) equipped with a stirbar was added $Pd_2(dba)_3 \cdot CHCl_3$ (2 mol %), XPhos (8 mol %), sodium *tert*-butoxide (1.4 equiv), and the aryl bromide (1 equiv). Toluene (0.5 M) was added followed by the amine (1.2 equiv) and the reaction mixture was degassed by splurging with $N_{2(g)}$ for 10 min. The reaction vessel was sealed with a Teflon screw-cap, and lowered into a pre-heated 110 °C oil-bath. After 18-20 h, the reaction mixture was allowed to cool to r.t. and diluted with ethyl acetate. The reaction mixture was then concentrated *in vacuo*, and purified as specified.

General Procedure E: Saponification. To a 16 × 150 mm test tube equipped with a stirbar was added the ester (1 equiv), THF (0.24 M), H_2O (1.2 M), and lithium hydroxide (2 equiv). The reaction mixture was stirred at r.t. for 16-18 h, at which time it was acidified to pH 1 with 1M $HCl_{(aq)}$. The reaction mixture was extracted with ethyl acetate (×4). The combined organic layers were washed with brine and concentrated *in vacuo* to give the desired products.

General Procedure F: Oxadiazole Formation. To an oven-dried round-bottom flask equipped with a stirbar was added the acid (1 equiv), EDC·HCl (1 equiv), HOBt (1 equiv), and DMF (0.8 M). The reaction mixture was stirred at r.t. for 30 min, at which time the amidoxime (1 equiv) was added. A reflux condenser was equipped and the reaction vessel was placed in a pre-heated 120-140 °C oil-bath and stirred overnight (14-18 h). The reaction mixture was cooled to r.t., diluted with EtOAc and water. The layers were separated, and the aqueous layer was extracted with EtOAc (×1). The combined organic layers were washed with water, 1M $HCl_{(aq)}$, water, brine, dried over $MgSO_4$, and concentrated *in vacuo* to give the desired product.

General Procedure G: Reductive Amination. To a round-bottom flask equipped with a stirbar was added the aldehyde (1 equiv), amine (1.05 equiv), methanol (0.07 M), and acetic acid (2 M). The reaction mixture was stirred for 30 min at which time sodium cyanoborohydride (0.5 equiv) was added as a solution in methanol (0.25 M). The reaction mixture was stirred for 1-2 h, at which time the solids were filtered and washed with methanol to give the desired product.

4-(2-Fluoroethoxy)-3-(trifluoromethyl)benzoic acid (7a) To an oven-dried 500 mL round-bottom flask equipped with a stirbar was added 4-fluoro-3-(trifluoromethyl)benzoic acid (**8**)(8.32 g, 40.0 mmol), 100 mL DMSO and 2-fluoroethanol (3.52 mL, 60.0 mmol). Sodium hydride (3.60 g, 90.0 mmol) was added portionwise, and the reaction mixture was stirred for 16 h. The reaction mixture was poured into water, and acidified with 12 M $HCl_{(aq)}$ to pH = 1. The resulting precipitate was filtered, washed with water and hexanes to give a tan solid (9.8 g, 97% yield). ^{1}H NMR (400 MHz, DMSO-d6) δ = 12.18 (s, 1H), 8.18 (dd, *J* = 8.8 Hz, 2.0 Hz, 1H), 8.11 (d, *J* = 2.0 Hz, 1H), 7.39 (d, *J* = 8.8 Hz, 1H), 4.85 – 4.40 (m, 4H) ^{13}C NMR (101 MHz, DMSO-d6) δ = 166.0, 159.44, 135.6, 128.0 (q, J_{C-F} = 4.9 Hz), 123.2 (q, J_{C-F} = 274 Hz), 123.2, 117.4 (q, J_{C-F} = 31.1 Hz), 113.9, 81.8 (d, J_{C-F} = 168 Hz), 68.6 (d, J_{C-F} = 19.1 Hz) MP: 131-133 °C HRMS (EI-TOF) m/z calcd for $C_{10}H_7F_4O_3$ [M-H] 251.0337. Found [M-H] 251.0289.

4'-Fluoro-2-(trifluoromethyl)-[1,1'-biphenyl]-4-carboxylic acid (7b). Following general experimental procedure A: $Pd(OAc)_2$ (67 mg, 0.30 mmol), SPhos (306 mg, 0.75 mmol), **6** (4.0 g, 14.9 mmol), 4-fluorophenylboronic acid (2.29 mg, 16.4 mmol), cesium fluoride (6.79 g, 44.7 mmol), 1,4-dioxane (40 mL), and degassed H_2O (40 mL) were combined. The reaction mixture was stirred for 18 h, to give 3.0 g of a tan solid which was used without further purification. ^{1}H NMR (400 MHz, DMSO-d6) δ = 13.56 (br s, 1H), 8.28 (s, 1H), 8.23 (d, *J* = 8 Hz, 1H), 7.57 (d, *J* = 8 Hz, 1H), 7.43 – 7.38 (m, 2H), 7.35 – 7.29 (m, 2H).

2'-Hydroxy-2-(trifluoromethyl)-[1,1'-biphenyl]-4-carboxylic acid (7c). Following general experimental procedure A: $Pd(OAc)_2$ (84 mg, 0.37 mmol), SPhos (382 mg, 0.93 mmol), **6** (5.0 g, 18.6 mmol), 2-hydroxyphenylboronic acid (2.82 g, 20.4 mmol), cesium fluoride (8.48 g, 55.8 mmol), 1,4-dioxane (50 mL) and degassed H_2O (50 mL) were combined. The reaction mixture was stirred for 20 h, and purified on a silica gel column, eluting with 5% MeOH/ CH_2Cl_2, to provide 5.2 g of a yellow semi-solid. ^{1}H NMR (400 MHz, DMSO-d6) δ = 9.54 (s, 1H), 8.25 (s, 1H), 8.18 (d, *J* = 8 Hz, 1H), 7.47 (d, *J* = 8 Hz, 1H), 7.23 (td, *J* = 8.8 Hz, 1.6 Hz, 1H), 7.04 (d, *J* = 7.2 Hz, 1H), 6.91 (d, *J* = 8.4 Hz, 1H), 6.85 (t, *J* = 7.2 Hz, 1H).

4'-Hydroxy-2-(trifluoromethyl)-[1,1'-biphenyl]-4-carboxylic acid (7d). Following general experimental procedure A: $Pd(OAc)_2$ (67 mg, 0.30 mmol), SPhos (306 mg, 0.75 mmol), **6** (4.0 g, 14.9 mmol), 4-hydroxyphenylboronic acid (2.46 mg, 17.8 mmol), cesium fluoride (6.79 g, 44.7 mmol), 1,4-dioxane (40 mL) and degassed H_2O (40 mL). The reaction

mixture was stirred for 20 h, and purified on a silica gel column, eluting with 5% MeOH / CH_2Cl_2, to provide 4.2 g of a yellow semi-solid. ^{1}H NMR (400 MHz, DMSO-d6) δ = 9.73 (s, 1H), 8.25 (s, 1H), 8.18 (d, *J* = 8 Hz, 1H), 7.52 (d, *J* = 8 Hz, 1H), 7.16 (d, *J* = 8.4 Hz, 2H), 6.83(d, *J* = 8.8 Hz, 2H).

2,4'-Bis(trifluoromethyl)-[1,1'-biphenyl]-4-carboxylic acid (7e). Following general experimental procedure A: $Pd(OAc)_2$ (42 mg, 0.19 mmol), SPhos (191 mg, 0.47 mmol), **6** (2.5 g, 9.3 mmol), 4-(trifluorofluoromethyl)phenylboronic acid (2.12 g, 11.2 mmol), potassium fluoride (4.24 g, 27.9 mmol), 1,4-dioxane (25 mL), and degassed H_2O (25 mL). The reaction mixture was stirred for 22 h, to give 2.35 g of a yellow solid, which was used without further purification. ^{1}H NMR (400 MHz, DMSO-d6) δ = 12.67 (br s, 1H), 8.31 (d, *J* = 1.2 Hz, 1H), 8.26 (d, *J* = 8 Hz, 1H), 7.85 (d, *J* = 8.4 Hz, 2H), 7.61 (t, *J* = 7.6 Hz, 3H).

4-(6-Fluoropyridin-3-yl)-3-(trifluoromethyl)benzoic acid (7f). Following general experimental procedure A: $Pd(OAc)_2$ (50 mg, 0.22 mmol), SPhos (230 mg, 0.56 mmol), **6** (3.0 g, 11.15 mmol), (6-fluoropyridin-3-yl)boronic acid (1.89 g, 13.4 mmol), cesium fluoride (5.08 g, 33.5 mmol), 30 mL 1,4-dioxane, and 30 mL degassed H_2O. The reaction mixture was stirred for 18h, to give a yellow solid, which was used without further purification (3.0 g, 94% yield). ^{1}H NMR (400 MHz, DMOS-d6) δ = 13.63 (br s, 1H), 8.31 (s, 1H), 8.30 – 8.24 (m, 2H), 8.09 – 7.98 (m, 1H), 7.66 (d, *J* = 7.6 Hz), 7.34 (dd, *J* = 8.4 Hz, 2.8 Hz, 1H).

3'-Methoxy-2-(trifluoromethyl)-[1,1'-biphenyl]-4-carboxylic acid (7g). Following general experimental procedure A: $Pd(OAc)_2$ (50 mg, 0.22 mmol), SPhos (230 mg, 0.56 mmol), **6** (3.0 g, 11.15 mmol), 3-methoxyphenylboronic acid (2.04 g, 13.4 mmol), cesium fluoride (5.08 g, 33.5 mmol), 30 mL 1,4-dioxane, and 30 mL degassed H_2O. The reaction mixture was stirred for 18 h, to give a yellow solid, which was used without further purification (3.12 g, 95% yield). ^{1}H NMR (400 MHz, DMSO-d6) δ = 13.22 (br s, 1H), 8.28 (d, *J* = 1.2 Hz, 1H), 8.22 (dd, *J* = 8.0 Hz, 1.6 Hz, 1H), 7.57 (d, *J* = 8.0 Hz, 1H), 7.38 (t, *J* = 8.4 Hz, 1H), 7.06 – 7.01 (m, 1H), 6.93 – 6.86 (m, 2H), 3.78 (s, 3H).

Methyl 3-amino-4-hydroxybenzoate (9). To a 250 mL round-bottom flask equipped with a stirbar was added methyl 4-hydroxy-3-nitrobenzoate (5.0 g, 25.4 mmol), 120 mL EtOH, and 540 mg 10% Pd/C. One balloon of $H_{2(g)}$ was bubbled through the reaction mixture, and then it was stirred under 1 atm of $H_{2(g)}$ overnight (16 h). At this time the reaction was filtered through a Celite plug, washing with EtOH, and concentrated *in vacuo* to give a brown solid (4.17 g, 98% yield). ^{1}H NMR (400 MHz, $CDCl_3$) δ = 7.45 (d, *J* = 2.0 Hz, 1H), 7.42 (dd, *J* = 8.0 Hz, 2.0 Hz, 1H), 7.75 (d, *J* = 8.4 Hz, 1H), 3.87 (s, 3H).

Methyl 3-(4-(2-fluoroethoxy)-3-(trifluoromethyl)benzamido)-4-hydroxybenzoate (10a). To an oven-dried 100 mL round-bottom flask equipped with a stirbar was added acid **7a** (2.50 g, 9.91 mmol), 50 mL CH_2Cl_2 and 10 drops of DMF. Oxalyl chloride (1.68 mL, 19.8 mmol) was added carefully and the reaction mixture was stirred for 2h at r.t. The reaction was concentrated *in vacuo* and dissolved in 33 mL CH_2Cl_2. Triethylamine (5.52 mL, 39.6 mmol) was added followed by DMAP (120 mg, 0.99 mmol), and aniline **9a** (1.66 g, 9.91 mmol). The reaction mixture was stirred overnight and diluted with MTBE, at which point a precipitate had formed. The precipitate was filtered, washed with MTBE and hexanes to give a white solid which was used in the next step without further purification. ^{1}H NMR (400 MHz, DMSO-d6) δ = 10.75 (br s, 1H), 9.83 (s, 1H), 8.27 (app q, *J* = 2.4 Hz, 2H), 8.23 (d, *J* = 2.4 Hz, 1H), 7.70 (dd, *J* = 8.4 Hz, 2.4 Hz, 1H), 7.43 (d, *J* = 9.2 Hz, 1H), 7.02 (d, *J* = 8.4 Hz, 1H), 4.87 – 4.68 (m, 2H), 4.57 – 4.42 (m, 2H).

***N*-(5-Bromo-2-hydroxyphenyl)-4'-fluoro-2-(trifluoromethyl)-[1,1'-biphenyl]-4-carboxamide (10b)**. Following general experimental procedure B: Carboxylic acid **7b** (720 mg, 2.53 mmol), 25.3 mL CH_2Cl_2, oxalyl chloride (0.49 mL, 5.82 mmol), 17 mL toluene, 8.5 mL of 10% $NaHCO_{3(aq)}$, **9b** (476 mg, 2.53 mmol) were combined to give amide **10b** as a tan solid (1.11 g, 99% yield). ^{1}H NMR (400 MHz, DMSO-d6) δ = 8.30 (s, 1H), 8.19 (d, *J* = 8 Hz, 1H), 7.99 (s, 1H), 7.51 (d, *J* = 8 Hz, 1H), 7.35 – 7.25 (m, 4H), 7.08 (d, *J* = 8 Hz, 1H), 6.76 (d, *J* = 8 Hz, 1H).

***N*-(5-Bromo-2-hydroxyphenyl)-2'-hydroxy-2-(trifluoromethyl)-[1,1'-biphenyl]-4-carboxamide (10c)**. Following general experimental procedure B: Carboxylic acid **7c** (3.5 g, 12.4 mmol), 124 mL CH_2Cl_2, oxalyl chloride (2.41 mL, 28.5 mmol) , 82 mL toluene, 41 mL of 10% $NaHCO_{3(aq)}$, and **9b** (2.33 g, 12.4 mmol) were combined to give amide **10c** as a brown solid (1.15 g, 20% yield). ^{1}H NMR (400 MHz, DMSO-d6) δ = 8.32 (s, 1H), 8.19 (d, *J* = 8.0 Hz, 1H), 7.87 (d, *J* = 2.4 Hz, 1H), 7.48 (d, *J* = 7.6 Hz, 1H), 7.28 – 7.17 (m, 2H), 7.05 (d, *J* = 6.8 Hz, 1H), 6.92 (d, *J* = 8.0 Hz, 1H), 6.89 – 6.82 (m, 2H).

***N*-(5-Bromo-2-hydroxyphenyl)-4'-hydroxy-2-(trifluoromethyl)-[1,1'-biphenyl]-4-carboxamide (10d)**. Following general experimental procedure B: Carboxylic acid **7d** (4.2 g, 14.9 mmol), 149 mL CH_2Cl_2, oxalyl chloride (2.90 mL, 34.3 mmol), 100 mL toluene, 50 mL of 10% $NaHCO_{3(aq)}$, and **9b** (2.80 g, 14.9 mmol) were combined to give amide **10d** as a brown solid which was used in the next step without further purification (3.4 g, 50% yield).

***N*-(5-Bromo-2-hydroxyphenyl)-2,4'-bis(trifluoromethyl)-[1,1'-biphenyl]-4-carboxamide (10e)**. Following general experimental procedure B: Acid **7e** (2.27 g, 6.79 mmol), 68 mL CH_2Cl_2, oxalyl chloride (1.21 mL, 14.3 mmol), 46 mL toluene, 23 mL 10% $NaHCO_{3(aq)}$, and **9b** (1.28 g, 6.79 mmol) were combined to give a light brown solid (2.81 g, 82%

yield). ^{1}H NMR (400 MHz, DMSO-d6) δ = 10.09 (br s, 1H), 8.42 (s, 1H), 8.29 (d, *J* = 8.0 Hz, 1H), 7.92 – 7.84 (m, 3H), 7.65 – 7.56 (m, 3H), 7.23 (dd, *J* = 8.8 Hz, 2.4 Hz, 1H), 6.89 (d, *J* = 8.8 Hz, 1H).

***N*-(5-Bromo-2-hydroxyphenyl)-4-(6-fluoropyridin-3-yl)-3-(trifluoromethyl)benzamide (10f)**. Following general experimental procedure B: Acid **7f** (1.00 g, 3.51 mmol), 35 mL CH_2Cl_2, oxalyl chloride (0.68 mL, 8.1 mmol), 24 mL toluene, 12 mL 10% $NaHCO_{3(aq)}$, and **9b** (660 mg, 3.51 mmol) were combined to give a tan solid (1.0 g, 63% yield). ^{1}H NMR (400 MHz, DMSO-d6) δ = 10.32 (br s, 1H), 8.40 (s, 1H), 8.35 – 8.18 (m, 2H), 8.03 (t, *J* = 8.4 Hz, 1H), 7.89 (d, *J* = 1.6 Hz, 1H), 7.64 (d, *J* = 7.6 Hz, 1H), 7.35 (d, *J* = 6.4 Hz, 1H), 7.19 (d, *J* = 8.4 Hz, 1H), 6.87 (d, *J* = 8.8 Hz, 1H).

Methyl 3-(4-(6-fluoropyridin-3-yl)-3-(trifluoromethyl)benzamido)-4-hydroxybenzoate (10g). To an oven-dried 100 mL round-bottom flask equipped with a stirbar was added acid **7f** (1.50 g, 5.26 mmol), 53 mL CH_2Cl_2 and ten drops of DMF. Oxalyl chloride (0.89 mL, 10.5 mmol) was added carefully, and the reaction was stirred for 2h, where upon it was concentrated *in vacuo* to give a yellow semi-solid. The crude acid chloride was suspended in 26 mL CH_2Cl_2 and triethylamine (2.93 mL, 21.0 mmol) was added, followed by DMAP (64 mg, 0.53 mmol). The reaction was stirred for 5 min at which time aniline **9a** (880 mg, 5.26 mmol) was added. The reaction mixture was stirred overnight (18 h), quenched with 1M $HCl_{(aq)}$ and diluted with CH_2Cl_2, causing a suspension to form in the organic layer. The layers were separated, and the aqueous layer was extracted with CH_2Cl_2 (×3). The combined organic layers were diluted with hexanes and filtered to give a brown solid (1.02 g, 45% yield). ^{1}H NMR (400 MHz, DMSO-d6) δ = 10.78 (br s, 1H), 10.05 (br s, 1H), 8.45 (s, 1H), 8.33 (d, *J* = 7.6 Hz, 1H), 8.29 (s, 2H), 8.05 (t, *J* = 6.4 Hz, 1H), 7.73 (d, *J* = 8.4 Hz, 1H), 7.68 (d, *J* = 8.0 Hz, 1H), 7.35 (d, *J* = 8.4 Hz, 1H), 7.04 (d, *J* = 8.4 Hz, 1H), 3.82 (s, 3H).

***N*-(5-Bromo-2-hydroxyphenyl)-3'-methoxy-2-(trifluoromethyl)-[1,1'-biphenyl]-4-carboxamide (10h)**. Following general experimental procedure B: Acid **7g** (3.1 g, 10.5 mmol), 105 mL CH_2Cl_2, oxalyl chloride (2.04 mL, 24.2 mmol), 70 mL toluene, 35 mL 10% $NaHCO_{3(aq)}$, and **9b** (1.97 g, 10.5 mmol) were combined to give a brown solid which was used in the next step without further purification (3.96 g, 81% yield).

Methyl 2-(4-(2-fluoroethoxy)-3-(trifluoromethyl)phenyl)benzo[d]oxazole-5-carboxylate (11a). Following general experimental procedure C: Amide **10a** (crude from previous step), 99 mL toluene and *p*-toluenesulfonic acid (3.77 g, 19.8 mmol) were combined to give a tan solid (1.1 g, 29% yield over two steps). ^{1}H NMR (400 MHz, $CDCl_3$) δ = 8.56 – 8.49 (m, 1H), 8.45 (d, *J* = 1.6 Hz, 1H), 8.41 (dd, *J* = 8.8 Hz, 2.4 Hz, 1H), 8.12 (dd, *J* = 8.4 Hz, 1.6 Hz, 1H), 7.62 (d, *J* = 8.4 Hz, 1H), 7.17 (d, *J* = 8.4 Hz, 1H), 4.93 – 4.75 (m, 2H), 4.48 – 4.37 (m, 2H), 3.97 (s, 3H).

5-Bromo-2-(4'-fluoro-2-(trifluoromethyl)-[1,1'-biphenyl]-4-yl)benzo[d]oxazole (11b). Following general experimental procedure C: Amide **10b** (980 mg, 2.17 mmol), 21.7 mL toluene, and *p*-toluenesulfonic acid (867 mg, 4.56 mmol) were combined to give oxazole **11b** as a red solid (760 mg, 80% yield). ^{1}H NMR (400 MHz, DMSO-d6) δ = 8.52 (s, 1H), 8.48 (d, *J* = 8 Hz, 1H), 8.13 (d, *J* = 2 Hz, 1H), 7. 86 (d, *J* = 8.8 Hz, 1H), 7.69 (d, *J* = 8 Hz, 1H), 7.66 (dd, *J* = 8.8 Hz, 2 Hz, 1H), 7.50 – 7.41 (m, 2H), 7.35 (t, *J* = 8.8 Hz, 2H).

5-Bromo-2-(2'-(2-fluoroethoxy)-2-(trifluoromethyl)-[1,1'-biphenyl]-4-yl)benzo[d]oxazole (11c). Following general experimental procedure C: Amide **10c** (1.06 g, 2.34 mmol), 23.4 mL toluene, and *p*-toluenesulfonic acid (0.94 g, 4.92 mmol) were combined to give the crude product which was applied to a silica gel column, eluted with 20% EtOAc/ hexanes, to provide the phenol intermediate as a red solid (820 mg, 80% yield). ^{1}H NMR (400 MHz, DMSO-d6) δ = 9.64 (s, 1H), 8.49 (s, 1H), 8.43 (d, *J* = 8.0 Hz, 1H), 8.13 (d, *J* = 1.6 Hz, 1H), 7.86 (d, *J* = 8.4 Hz, 1H), 7.65 (dd, *J* = 8.8 Hz, 2.0 Hz, 1H), 7.60 (d, *J* = 8.8 Hz, 1H), 7.26 (t, *J* = 7.6 1H), 7.09 (d, *J* = 7.2 Hz, 1H), 6.94 (d, *J* = 8.4 Hz, 1H), 6.87 (t, *J* = 7.2 Hz, 1H).

To an oven-dried 16 × 125 mm test tube equipped with a stirbar was added the phenol prepared above (290 mg, 0.67 mmol), cesium carbonate (437 mg, 1.34 mmol) and 2.2 mL *N,N*-dimethylformamide. 2-Fluoroethyl 4-methylbenzenesulfonate (160 mg, 0.73 mmol) was added via syringe and the reaction vessel was placed in a pre-heated 70 °C oil-bath and stirred for 4 h. The reaction mixture was cooled to r.t., diluted with EtOAc and H_2O, and the layers were separated. The organic layer was washed with H_2O (×5) and brine, dried over sodium sulfate, and concentrated *in vacuo* to give a light brown solid, which was used without further purification (310 mg, 97% yield). ^{1}H NMR (400 MHz, $CDCl_3$) δ = 8.58 (s, 1H), 8.34 (d, *J* = 8.4 Hz, 1H), 7.89 (s, 1H), 7.53 – 7.43 (m, 3H), 7.38 (t, *J* = 7.6 Hz, 1H), 7.20 (d, *J* = 7.2 Hz, 1H), 7.04 (t, *J* = 7.6 Hz, 1H), 6.95 (d, *J* = 8.4 Hz, 1H), 4.52 (dt, *J* = 47.2 Hz, 4 Hz, 2H), 4.31 – 4.03 (m, 2H).

5-Bromo-2-(4'-(2-fluoroethoxy)-2-(trifluoromethyl)-[1,1'-biphenyl]-4-yl)benzo[*d*]oxazole (11d). Following general experimental procedure C: Amide **10d** (3.4 g, 7.52 mmol), 75 mL toluene, and *p*-toluenesulfonic acid (3.0 g, 15.8 mmol) were combined to give the crude product, which was applied to a silica gel column, eluted with 20% EtOAc/ hexanes, to provide the phenol intermediate as a red solid (1.21 g, 37% yield). ^{1}H NMR (400 MHz, DMSO-d6) δ = 9.77 (s, 1H), 8.46 (s, 1H), 8.41 (d, *J* = 8 Hz, 1H), 8.10 (d, *J* = 1.6 Hz, 1H), 7.83 (d, *J* = 8.8 Hz, 1H), 7.63 (d, *J* = 8 Hz, 1H), 7.66 (dd, *J* = 8.8 Hz, 2 Hz, 1H), 7.20 (d, *J* = 8.4 2H), 7.86 (d, *J* = 8.4 Hz, 2H).

To an oven-dried 16 × 125 mm test tube equipped with a stirbar was added the phenol prepared above (217 mg, 0.50 mmol), cesium carbonate (326 mg, 1.0 mmol) and 1.7 mL *N,N*-dimethylformamide. 2-Fluoroethyl 4-

methylbenzenesulfonate (120 mg, 0.55 mmol) was added via syringe and the reaction vessel was placed in a pre-heated 70 °C oil-bath and stirred for 4 h. The reaction mixture was cooled to r.t., diluted with EtOAc and H_2O, and the layers were separated. The organic layer was washed with H_2O (×5) and brine, dried over sodium sulfate, and concentrated *in vacuo* to give 232 mg of a light brown solid, which was used without further purification. ^{1}H NMR (400 MHz, DMSO-d6) δ = 8.51 (s, 1H), 8.46 (d, *J* = 8 Hz, 1H), 8.13 (d, *J* = 2 Hz, 1H), 7.86 (d, *J* = 8.4 Hz, 1H), 7.70 – 7.62 (m, 2H), 7.34 (d, *J* = 8.4 Hz, 2H), 7.09 (d, *J* = 8.8 Hz, 2H), 4.87 – 4.70 (m, 2H), 4.37 – 4.25 (m, 2H).

2-(2,4'-Bis(trifluoromethyl)-[1,1'-biphenyl]-4-yl)-5-bromobenzo[*d*]oxazole (11e). Following general experimental procedure C: Amide **10e** (2.70 g, 5.35 mmol), 54 mL toluene, and *p*-toluenesulfonic acid monohydrate (2.14 g, 11.2 mmol) were combined to give a light red solid (2.39 g, 92 % yield). ^{1}H NMR (400 MHz, DMSO-d6) δ = 8.55 (s, 1H), 8.52 (d, *J* = 8.0 Hz, 1H), 8.15 (d, *J* = 2.0 Hz, 1H), 7.92 – 7.85 (m, 3H), 7.75 (d, *J* = 8.4 Hz, 1H), 7.69 – 7.61 (m, 3H).

5-Bromo-2-(4-(6-fluoropyridin-3-yl)-3-(trifluoromethyl)phenyl)benzo[*d*]oxazole (11f). To an oven-dried 25 mL round-bottom flask equipped with a stirbar was added amide **10f** (935 mg, 2.05 mmol) and 8.2 mL THF. Triphenylphosphine (1.19 g, 4.52 mmol) was added followed by diisopropylazodicarboxylate (0.89 mL, 4.52 mmol). The reaction mixture was stirred at r.t. for 22 h, and concentrated *in vacuo*. The crude product was diluted with diethyl ether, and filtered through a Celite plug, washing with ether. The ether mixture was concentrated *in vacuo* and applied to a silica gel column, eluting with 15% EtOAc/ hexanes to give a pink solid (500 mg, 56% yield). ^{1}H NMR (400 MHz, $CDCl_3$) δ = 8.66 (d, *J* = 1.2 Hz, 1H), 8.46 (dd, *J* = 8.0 Hz, 1.6 Hz, 1H), 8.24 (d, *J* = 2.0 Hz, 1H), 7.82 (td, *J* = 8.0 Hz, 2.4 Hz, 1H), 7.55 – 7.47 (m, 3H), 7.04 (dd, *J* = 8.4 Hz, 2.8 Hz, 1H).

Methyl 2-(4-(6-fluoropyridin-3-yl)-3-(trifluoromethyl)phenyl)benzo[*d*]oxazole-5-carboxylate (11g). Following general experimental procedure C: Amide **10g** (500 mg, 1.15 mmol), 11.5 mL toluene, and pyridinium *p*-toluenesulfonate (607 mg, 2.42 mmol) were combined to give a yellow solid (415 mg, 87% yield). ^{1}H NMR (400 MHz, $CDCl_3$) δ = 8.64 (d, *J* = 1.2 Hz, 1H), 8.48 – 8.42 (m, 2H), 8.22 (d, *J* = 2.0 Hz, 1H), 8.13 (dd, *J* = 8.4 Hz, 1.6 Hz, 1H), 7.81 (td, *J* = 8.0 Hz, 2.4 Hz, 1H), 7.64 (d, *J* = 8.4 Hz, 1H), 7.50 (d, *J* = 8.0 Hz, 1H), 7.03 (dd, *J* = 8.4 Hz, 2.8 Hz, 1H), 3.96 (s, 3H).

5-Bromo-2-(3'-methoxy-2-(trifluoromethyl)-[1,1'-biphenyl]-4-yl)benzo[*d*]oxazole (11h). Following general experimental procedure C: Amide **10h** (3.96 g, 8.49 mmol), 85 mL toluene, and *p*-toluenesulfonic acid (3.39 g, 17.8 mmol) were combined to give a red solid (3.24 g, 85% yield). ^{1}H NMR (400 MHz, $CDCl_3$) δ = 8.61 (d, *J* = 1.6 Hz, 1H), 8.39 (dd, *J* = 8.0 Hz, 1.6 Hz, 1H), 7.96 – 7.93 (m, 1H), 7.57 – 7.49 (m, 3H), 7.36 (t, *J* = 7.6 Hz, 1H), 7.02 – 6.90 (m, 3H), 3.85 (s, 3H).

(2-(4-(6-Fluoropyridin-3-yl)-3-(trifluoromethyl)phenyl)benzo[*d*]oxazol-5-yl)methanol (12a). To a 25 mL round-bottom flash equipped with a stirbar was added ester **11g** (415 mg, 0.99 mmol) and 5 mL THF. The reaction was cooled in a - 78°C cooling bath ($CO_{2(s)}$ / acetone) and DIBAl-H (2.99 mL, 2.99 mmol, 1.0 M in hexanes) was added slowly. The reaction was allowed to warm in the bath to - 15°C for 1 h, at which time TLC indicated consumption of the starting ester. The reaction was quenched with 2 mL EtOAc and 5 mL saturated Rochelle's salt solution and stirred 30 min. The reaction mixture was diluted with EtOAc, and the layers separated. The aqueous layer was extracted with EtOAc (×2). The combined organic layers were washed with H_2O, brine, dried over $MgSO_4$, and concentrated *in vacuo* to give a white solid (350 mg, 91% yield). ^{1}H NMR (400 MHz, $CDCl_3$) δ = 8.69 (s, 1H), 8.48 (dd, *J* = 8.0 Hz, 1.6 Hz, 1H), 8.24 (d, *J* = 2.0 Hz, 1H), 7.86 – 7.78 (m, 2H), 7.62 (d, *J* = 8.4 Hz, 1H), 7.51 (d, *J* = 8.0 Hz, 1H), 7.45 (dd, *J* = 8.4 Hz, 1.6 Hz, 1H), 7.04 (dd, *J* = 8.4 Hz, 3.2 Hz, 1H), 4.86 (s, 2H).

(2-(4-(2-Fluoroethoxy)-3-(trifluoromethyl)phenyl)benzo[*d*]oxazol-5-yl)methanol (12b). To an oven-dried 50 mL round-bottom flask equipped with a stirbar was added ester **11a** (844 mg, 2.2 mmol) and 11 mL 2-methyltetrahydrofuran. The reaction mixture was cooled to -78 °C ($CO_{2(s)}$/acetone bath) and DIBAl-H (1.0 M solution in hexanes, 6.6 mL, 6.6 mmol) was added carefully. The reaction mixture was allowed to warm to -5 °C in the bath over 1 h, at which time TLC showed consumption of the ester. The reaction was quenched with EtOAc and sat. Rochelle's salt solution$_{(aq)}$, and stirred for 30 min when a precipitate had formed. The reaction mixture was filtered through a Celite plug, washing with EtOAc and water. The layers were separated and the aqueous layer was extracted with EtOAc (×1). The combined organic layers were washed with water, brine, dried over $MgSO_4$, and concentrated *in vacuo* to give a white solid (743 mg, 95% yield). ^{1}H NMR (400 MHz, $CDCl_3$) δ = 8.48 (d, *J* = 2.0 Hz, 1H), 8.37 (dd, *J* = 8.8 Hz, 2.0 Hz, 1H), 7.74 (s, 1H), 7.55 (d, *J* = 8.4 Hz, 1H), 7.40 – 7.35 (m, 1H), 7.14 (d, *J* = 8.8 Hz, 1H), 4.90 – 4.74 (m, 2H), 4.82 (s, 2H), 4.47 – 4.35 (m, 2H).

5-(Chloromethyl)-2-(4-(6-fluoropyridin-3-yl)-3-(trifluoromethyl)phenyl)benzo[*d*]oxazole (13a). To an oven-dried 10 mL round-bottom flask equipped with a stirbar was added 0.11 mL DMF, followed by cyanuric chloride (194 mg, 1.05 mmol). The reaction was stirred for 30 min, at which time TLC analysis showed consumption of the cyanuric chloride. 2.5 mL CH_2Cl_2 was added, followed by alcohol **12a** (388 mg, 1.00 mmol). The reaction was stirred for 1 h, at which time TLC analysis showed consumption of the alcohol. The reaction was quenched with H_2O and diluted with CH_2Cl_2. The layers were separated, and the aqueous layer was extracted with CH_2Cl_2 (× 1). The combined organic layers were washed with saturated sodium carbonate solution, 1M $HCl_{(aq)}$, brine, dried over $MgSO_4$ and concentrated *in vacuo* to give 398 mg of an off-white solid. ^{1}H NMR (400 MHz, $CDCl_3$) δ = 8.68 (s, 1H), 8.48 (d, *J* = 8.0 Hz, 1H), 8.24 (d, *J* = 2.0 Hz, 1H), 7.86

– 7.77 (m, 2H), 7.63 (d, *J* = 8.4 Hz, 1H), 7.52 (d, *J* = 8.0 Hz, 1H), 7.47 (dd, *J* = 8.4 Hz, 1.6 Hz, 1H), 7.04 (dd, *J* = 8.4 Hz, 2.4 Hz, 1H), 4.75 (s, 2H).

5-(Chloromethyl)-2-(4-(2-fluoroethoxy)-3-(trifluoromethyl)phenyl)benzo[*d*]oxazole (13b). To an oven-dried 50 mL round-bottom flask equipped with a stirbar was added 0.23 mL DMF and cyanuric chloride (218 mg, 1.18 mmol). The reaction mixture was stirred for 1 h at which time 3 mL CH_2Cl_2 and alcohol **12b** (400 mg, 1.13 mmol) were added. The reaction mixture was stirred for 18 h, diluted with CH_2Cl_2 and water. The layers were separated and the aqueous layer was extracted with CH_2Cl_2 (×2). The combined organic layers were washed with sat. $Na_2CO_{3(aq)}$, 1M HCl $_{(aq)}$, brine; dried over $MgSO_4$, and concentrated *in vacuo* to give a tan solid (250 mg, 59% yield). ^{1}H NMR (400 MHz, $CDCl_3$) δ = 8.47 (s, 1H), 8.38 (dd, *J* = 8.8 Hz, 2.4 Hz, 1H), 7.76 (s, 1H), 7.56 (d, *J* = 8.4 Hz, 1H), 7.40 (dd, *J* = 8.4 Hz, 1.6 Hz, 1H), 7.15 (d, *J* = 8.8 Hz, 1H), 4.92 – 4.74 (m, 2H), 4.73 (s, 2H), 4.48 – 4.36 (m, 2H).

Methyl 1-((2-(4-(6-fluoropyridin-3-yl)-3-(trifluoromethyl)phenyl)benzo[*d*]oxazol-5-yl)methyl)azetidine-3-carboxylate (14a). To a 10 mL round-bottom flask equipped with a stirbar was added chloride **13a** (260 mg, 0.64 mmol), methyl azetidine-3-carboxylate hydrochloride (146 mg, 0.96 mmol), 2.1 mL acetonitrile and potassium carbonate (265 mg, 1.92 mmol). The reaction was stirred 3h, at which time no progress was observed by TLC. *i*Pr_2NEt (0.33 mL, 1.92 mmol) was added and the reaction stirred 20 h at r.t. The reaction was diluted with water and EtOAc, and the layers separated. The aqueous layer was extracted with EtOAc (× 1). The combined organic layers were washed with water (×2), brine, dried over $MgSO_4$ and concentrated *in vacuo* to give a yellow semi-solid. The crude product was then purified on a silica gel column, eluting with EtOAc to give a white solid (110 mg, 35% yield). ^{1}H NMR (400 MHz, $CDCl_3$) δ = 8.63 (d, *J* = 1.2 Hz, 1H), 8.43 (dd, *J* = 8 Hz, 1.6 Hz, 1H), 8.21 (d, *J* = 2.0 Hz, 1H), 7.80 (td, *J* = 8.4 Hz, 2.4 Hz, 1H), 7.69 (d, *J* = 0.8 Hz, 1H), 7.54 (d, *J* = 8.4 Hz, 1H), 7.47 (d, *J* = 8.0 Hz, 1H), 7.33 (dd, *J* = 8.4 Hz, 1.6 Hz, 1H), 7.01 (dd, *J* = 8.4 Hz, 3.2 Hz, 1H), 3.73 (s, 2H), 3.70 (s, 3H), 3.57 – 3.52 (m, 2H), 3.40 – 3.30 (m, 3H).

Methyl 1-((2-(4-(2-fluoroethoxy)-3-(trifluoromethyl)phenyl)benzo[*d*]oxazol-5-yl)methyl)azetidine-3-carboxylate (14b). To a 10 mL round-bottom flask equipped with a stirbar was added chloride **13b** (187 mg, 0.5 mmol), methyl azetidine-3-carboxylate hydrochloride (114 mg, 0.75 mmol), 1.7 mL MeCN, and DIPEA (0.26 mL, 1.5 mmol). The reaction was placed in a pre-heated 60 °C oil-bath and stirred overnight (~18 h). The reaction mixture was allowed to cool to r.t., diluted with water and EtOAc. The layers were separated, aqueous layer extracted with EtOAc (× 2). The combined organic layers were washed with water (× 3), brine, dried over $MgSO_4$, and concentrated *in vacuo* to give a tan solid (150 mg, 66% yield). ^{1}H NMR (400 MHz, $CDCl_3$) δ = 8.41 (s, 1H), 8.29 (d, *J* = 8.8 Hz, 1H), 7.60 (s, 1H), 7.44 (d, *J* = 8.4 Hz,

1H), 7.23 (d, *J* = 8.0 Hz, 1H), 7.07 (d, *J* = 8.8 Hz, 1H), 4.85 – 4.67 (m, 2H), 4.40 – 4.28 (m, 2H), 3.75 – 3.65 (m, 4H), 3.55 – 3.45 (m, 2H), 3.36 – 3.25 (m, 2H).

1-((2-(4-(6-Fluoropyridin-3-yl)-3-(trifluoromethyl)phenyl)benzo[*d*]oxazol-5-yl)methyl)azetidine-3-carboxylic acid (15a). To a 13 × 100 mm test-tube equipped with a stirbar was added ester **14a** (70 mg, 0.14 mmol), 1.1 mL THF, and 0.21 2M $LiOH_{(aq)}$. The reaction was stirred overnight at r.t., and quenched with 1M $HCl_{(aq)}$ to give a white precipitate. The precipitate was removed by filtration and dried under reduced pressure to provide 30 mg of the product. ^{1}H NMR (400 MHz, MeOD-d4) δ = 8.69 (s, 1H), 8.57 (dd, *J* = 8.0 Hz, 2.0 Hz, 1H), 8.23 (d, *J* = 2.0 Hz, 1H), 8.07 – 7.97 (m, 2H), 7.86 (d, *J* = 8.4 Hz, 1H), 7.71 (d, *J* = 8.0 Hz, 1H), 7.66 (d, *J* = 8.4 Hz, 1H), 7.22 (dd, *J* = 8.4 Hz, 2.8 Hz, 1H), 4.63 (d, *J* = 22.4 Hz, 2H), 4.48 (t, *J* = 10.4 Hz, 1H), 4.39 – 4.32 (m, 3H), 3.83 – 3.71 (m, 1H).

1-((2-(4-(2-Fluoroethoxy)-3-(trifluoromethyl)phenyl)benzo[*d*]oxazol-5-yl)methyl)azetidine-3-carboxylic acid (15b). To a 10 ml round-bottom flask equipped with a stirbar and containing ester **14b** (120 mg, 0.27 mmol) was added 2.1 ml THF and 0.4 ml 2M $LiOH_{(aq)}$. The reaction mixture was stirred overnight (18 h) and quenched with 1M $HCl_{(aq)}$. The reaction mixture was neutralized with sat. $NaHCO_{3(aq)}$ which caused the formation of a precipitate. This precipitate was filtered and washed with Et_2O to give a white solid (41 mg, 35% yield). ^{1}H NMR (400 MHz, MeOD-d4) δ = 8.50 – 8.43 (m, 2H), 7.90 (s, 1H), 7.80 (d, *J* = 8.4 Hz, 1H), 7.54 (d, *J* = 8.4 Hz, 1H), 7.45 (d, *J* = 9.6 Hz, 1H), 4.86 – 4.71 (m, 2H), 4.56 (d, *J* = 8.0 Hz, 2H), 4.54 – 4.25 (m, 6H), 3.72 (pent, *J* = 9.2 Hz, 1H).

5-(2-(4-(6-Fluoropyridin-3-yl)-3-(trifluoromethyl)phenyl)benzo[*d*]oxazol-5-yl)thiophene-2-carboxylic acid (16). To an oven-dried 25 mL Schlenk tube equipped with a stirbar was added palladium acetate (2.2 mg, 0.01 mmol), bromide **11f** (219 mg, 0.5 mmol), 2-carboxythiophene-5-boronic acid (95 mg, 0.55 mmol), cesium fluoride (228 mg, 1.5 mmol), 1.35 mL 1,4-dioxane, and 1.35 mL degassed H_2O. The reaction vessel was equipped with a cold-finger, placed in a pre-heated 110 °C oil-bath, and heated overnight (~18 h). The reaction was cooled to r.t. and poured into a 1:1 mixture of EtOAc/ 1M $HCl_{(aq)}$. The layers were separated, and the aqueous layer was extracted with EtOAc (×3). The combined organic layers were washed with brine, dried over Na_2SO_4, and concentrated *in vacuo* to give a brown solid (223 mg, 92% yield). ^{1}H NMR (400 MHz, DMSO-d6) δ = 13.19 (br s, 1H), 8.57 (s, 1H), 8.54 (d, *J* = 8.0 Hz, 1H), 8.31 (d, *J* = 2.4 Hz, 1H), 8.26 (d, *J* = 2.0 Hz, 1H), 8.09 (td, *J* = 8.0 Hz, 2.4 Hz, 1H), 7.95 (d, *J* = 8.8 Hz, 1H), 7.86 (dd, *J* = 8.8 Hz, 2.0 Hz, 1H), 7.79 (d, *J* = 8.0 Hz, 1H), 7.75 (d, *J* = 3.6 Hz, 1H), 7.68 (d, *J* = 4.0 Hz, 1H), 7.37 (dd, *J* = 8.8 Hz, 2.8 Hz, 1H).

Methyl 1-(2-(4'-fluoro-2-(trifluoromethyl)-[1,1'-biphenyl]-4-yl)benzo[*d*]oxazol-5-yl)piperidine-4-carboxylate (17a). Following general experimental procedure D: $Pd_2(dba)_3 \cdot CHCl_3$ (10 mg, 0.01 mmol), XPhos (19 mg, 0.040 mmol), sodium

tert-butoxide (67 mg, 0.70 mmol), oxazole **11b** (218 mg, 0.5 mmol), toluene (1 mL), methyl piperidine-4-carboxylate (81 µL, 0.60 mmol) were combined to give the crude product which was applied to a silica gel column, eluting with 5-15% ethyl acetate in hexanes to give ester **17a** as a yellow solid (165 mg, 66% yield). ^{1}H NMR (400 MHz, $CDCl_3$) δ = 8.59 (s, 1H), 8.36 (d, *J* = 8.0 Hz, 1H), 7.47 (d, *J* = 6.0 Hz, 1H), 7.44 (d, *J* = 4.4 Hz, 1H), 7.37 – 7.27 (m, 3H), 7.11 (t, *J* = 8.4 Hz, 2H), 7.07 (dd, *J* = 8.8 Hz, 2.4 Hz, 1H), 3.71 (s, 3H), 3.61 (dt, *J* = 8.8 Hz, 3.2 Hz, 2H), 2.82 (td, *J* = 12 Hz, 2.0 Hz, 2H), 2.47 (tt, *J* = 11.2 Hz, 4 Hz, 1H), 2.13 – 2.02 (m, 2H), 2.01 – 1.87 (m, 2H).

Methyl 1-(2-(2'-(2-fluoroethoxy)-2-(trifluoromethyl)-[1,1'-biphenyl]-4-yl)benzo[*d*]oxazol-5-yl)piperidine-4-carboxylate (17b). Following general experimental procedure D: $Pd_2(dba)_3{\cdot}CHCl_3$ (6.2 mg, 0.006 mmol), XPhos (11.4 mg, 0.024 mmol), sodium *tert*-butoxide (40 mg, 0.42 mmol), oxazole **11c** (144 mg, 0.30 mmol), toluene (0.6 mL), and methyl piperidine-4-carboxylate (48 µL, 0.36 mmol) were combined to give the crude product which was applied to a silica gel column, eluting with 20% ethyl acetate in hexanes to give ester **17b** as a yellow solid (90 mg, 56% yield). ^{1}H NMR (400 MHz, $CDCl_3$) δ = 8.60 (s, 1H), 8.37 (d, *J* = 8.0 Hz, 1H), 7.47 (dd, *J* = 9.2 Hz, 4.0 Hz, 2H), 7.39 (t, *J* = 7.6 Hz, 1H), 7.32 (br s, 1H), 7.21 (d, *J* = 7.2 Hz, 1H), 7.13 – 7.01 (m, 2H), 6.97 (d, *J* = 8.4 Hz, 1H), 4.54 (dt, *J* = 47.6 Hz, 4.0 Hz, 2H), 4.29 – 4.04 (m, 2H), 3.72 (s, 3H), 3.62 (d, *J* = 12.4 Hz, 2H), 2.84 (t, *J* = 11.2 Hz, 2H), 2.53 – 2.44 (m, 1H), 2.14 – 2.04 (m, 2H), 2.03 – 1.85 (m, 2H).

Methyl 1-(2-(4'-(2-fluoroethoxy)-2-(trifluoromethyl)-[1,1'-biphenyl]-4-yl)benzo[*d*]oxazol-5-yl)piperidine-4-carboxylate (17c). Following general experimental procedure D: $Pd_2(dba)_3{\cdot}CHCl_3$ (7.2 mg, 0.007 mmol), XPhos (13 mg, 0.028 mmol), sodium *tert*-butoxide (47 mg, 0.49 mmol), oxazole **11d** (168 mg, 0.35 mmol), toluene (0.7 mL), and methyl piperidine-4-carboxylate (57 µL, 0.42 mmol) were combined to give the crude product, applied to a silica gel column, eluting with 20% ethyl acetate in hexanes to give ester **17c** as a yellow solid (95 mg, 50% yield). ^{1}H NMR (400 MHz, $CDCl_3$) δ = 8.59 (s, 1H), 8.36 (d, *J* = 8.0 Hz, 1H), 7.47 (d, *J* = 6.0 Hz, 1H), 7.44 (d, *J* = 4.4 Hz, 1H), 7.37 – 7.27 (m, 3H), 7.11 (t, *J* = 8.4 Hz, 2H), 7.07 (dd, *J* = 8.8 Hz, 2.4 Hz, 1H), 3.71 (s, 3H), 3.61 (dt, *J* = 8.8 Hz, 3.2 Hz, 2H), 2.82 (td, *J* = 12 Hz, 2.0 Hz, 2H), 2.47 (tt, *J* = 11.2 Hz, 4 Hz, 1H), 2.13 – 2.02 (m, 2H), 2.01 – 1.87 (m, 2H).

Methyl 1-(2-(2,4'-bis(trifluoromethyl)-[1,1'-biphenyl]-4-yl)benzo[*d*]oxazol-5-yl)piperidine-4-carboxylate (17d). Following general experimental procedure D: $Pd_2(dba)_3{\cdot}CHCl_3$ (21 mg, 0.02 mmol), XPhos (38 mg, 0.08 mmol), sodium *tert*-butoxide (135 mg, 1.4 mmol), bromide **11e** (486 mg, 1.0 mmol), and 2 mL toluene were combined to provide the crude product. This was applied to a silica gel column, eluting with 20% EtOAc/ hexanes to provide a yellow powder (265 mg, 48% yield). ^{1}H NMR (400 MHz, $CDCl_3$) δ = 8.63 (s, 1H), 8.41 (d, *J* = 8.0 Hz, 1H), 7.70 (d, *J* = 8.0 Hz, 2H),

7.52 – 7.45 (m, 4H), 7.31 (d, *J* = 2.4 Hz, 1H), 7.10 (dd, *J* = 8.8 Hz, 2.0 Hz, 1H), 3.73 (s, 3H), 3.63 (dt, *J* = 12.4 Hz, 3.2 Hz, 2H), 2.84 (td, *J* = 11.6 Hz, 2.4 Hz, 2H), 2.47 (tt, *J* = 10.8 Hz, 4.0 Hz, 1H), 2.13 – 2.04 (m, 2H), 2.02 – 1.87 (m, 2H).

Methyl 1-(2-(3'-methoxy-2-(trifluoromethyl)-[1,1'-biphenyl]-4-yl)benzo[*d*]oxazol-5-yl)piperidine-4-carboxylate (17e). Following general experimental procedure D: $Pd_2(dba)_3 \cdot CHCl_3$ (21 mg, 0.02 mmol), XPhos (38 mg, 0.08 mmol), sodium *tert*-butoxide (135 mg, 1.4 mmol), bromide **11h** (447 mg, 1.0 mmol), and 2 mL toluene were combined to provide the crude product. This was applied to a silica gel column, eluting with 20% EtOAc / hexanes to provide a yellow powder (93 mg, 18% yield). ^{1}H NMR (400 MHz, $CDCl_3$) δ = 8.60 (s, 1H), 8.36 (d, *J* = 8.0 Hz, 1H), 7.49 (t, *J* = 8.0 Hz, 2H), 7.38 – 7.29 (m, 2H), 7.08 (d, *J* = 8.4 Hz, 1H), 7.00 – 6.87 (m, 3H), 3.84 (s, 3H), 3.72 (s, 3H), 3.62 (d, *J* = 12.4 Hz, 2H), 2.84 (t, *J* = 10.8 Hz, 2H), 2.53 – 2.42 (m, 1H), 2.13 – 2.04 (m, 2H), 2.03 – 1.86 (m, 2H).

1-(2-(4'-Fluoro-2-(trifluoromethyl)-[1,1'-biphenyl]-4-yl)benzo[*d*]oxazol-5-yl)piperidine-4-carboxylic acid (18a). Following general experimental procedure E: Ester **17a** (150 mg, 0.30 mmol), 1.25 mL tetrahydrofuran, 0.25 mL H_2O, and lithium hydroxide (14 mg, 0.60 mmol) were combined to give carboxylic acid **18a** as an off-white pearly solid (129 mg, 89% yield). ^{1}H NMR (400 MHz, MeOD-d4) δ = 8.67 (s, 1H), 8.54 (d, *J* = 8.0 Hz, 1H), 8.18 (d, *J* = 2.0 Hz, 1H), 7.98 (d, *J* = 9.2 Hz, 1H), 7.78 (dd, *J* = 8.8 Hz, 2.4 Hz, 1H), 7.65 (d, *J* = 8 Hz, 1H), 7.41 (dd, *J* = 8.4 Hz, 5.2 Hz, 2H), 7.22 (t, *J* = 8.8 Hz, 2H), 3.93 – 3.74 (m, 4 H), 2.93 – 2.82 (m, 1H), 2.41 (dd, *J* = 15.2 Hz, 3.6 Hz, 2H), 2.32 – 2.16 (m, 2H).

1-(2-(2'-(2-Fluoroethoxy)-2-(trifluoromethyl)-[1,1'-biphenyl]-4-yl)benzo[*d*]oxazol-5-yl)piperidine-4-carboxylic acid (18b). Following general experimental procedure E: Ester **17b** (90 mg, 0.17 mmol), 0.70 mL tetrahydrofuran, 0.13 mL H_2O, and lithium hydroxide (8.0 mg, 0.332 mmol were combined to give carboxylic acid **18b** as an off-white pearly solid (82 mg, 94% yield). ^{1}H NMR (400 MHz, MeOD-d4) δ = 8.52 (s, 1H), 8.35 (d, *J* = 8.0 Hz, 1H), 7.64 (d, *J* = 8.4 Hz, 1H), 7.56 (s, 1H), 7.48 (d, *J* = 8.0 Hz, 1H), 7.45 – 7.31 (m, 2H), 7.16 (d, *J* = 7.2 Hz, 1H), 7.08 (d, *J* = 8.4 Hz, 1H), 7.03 (t, *J* = 7.2 Hz, 1H), 4.51 (d, *J* = 48 Hz, 2H), 3.31 – 3.05 (m, 2H), 3.68 (d, *J* = 12 Hz, 2H), 3.14 (t, *J* = 10.4 Hz, 2H), 2.59 (t, *J* = 10.4 Hz, 1H), 2.26 – 2.10 (m, 2H), 2.09 – 1.92 (m, 2H).

1-(2-(4'-(2-Fluoroethoxy)-2-(trifluoromethyl)-[1,1'-biphenyl]-4-yl)benzo[*d*]oxazol-5-yl)piperidine-4-carboxylic acid (18c). Following general experimental procedure E: Ester **17c** (90 mg, 0.166 mmol), 0.7 mL tetrahydrofuran, 0.13 mL H_2O, and lithium hydroxide (8.0 mg, 0.332 mmol) were combined to give carboxylic acid **18c** as a light tan solid (87 mg, 99% yield). ^{1}H NMR (400 MHz, MeOD-d4) δ = 8.64 (s, 1H), 8.50 (d, *J* = 7.6 Hz, 1H), 8.29 (s, 1H), 7.96 (d, *J* = 8.8 Hz, 1H), 7.83 (dd, *J* = 8.8 Hz, 2.0 Hz, 1H), 7.63 (d, *J* = 8.0 Hz, 1H), 7.32 (d, *J* = 8.4 Hz, 2H), 7.06 (d, *J* = 8.8 Hz, 2H), 4.77

(dt, *J* = 48 Hz, 4 Hz, 2H), 4.29 (dt, *J* = 28.8 Hz, 3.6 Hz, 2H), 3.90 – 3.74 (m, 4H), 2.93 – 2.83 (m, 1H), 2.49 – 2.35 (m, 2H), 2.35 – 2.20 (m, 2H).

1-(2-(2,4'-*Bis*(trifluoromethyl)-[1,1'-biphenyl]-4-yl)benzo[*d*]oxazol-5-yl)piperidine-4-carboxylic acid (18d). Following general experimental procedure E: Ester **17d** (102 mg, 0.19 mmol), 0.79 mL THF, and 0.16 mL H_2O. LiOH (8.9 mg, 0.37 mmol) were combined to give an off-white solid. (101 mg, 99% yield). ^{1}H NMR (400 MHz, MeOD-d4) δ = 8.70 (s, 1H), 8.58 (d, *J* = 8.0 Hz, 1H), 8.28 (d, *J* = 2.0 Hz, 1H), 7.99 (d, *J* = 9.2 Hz, 1H), 7.89 (dd, *J* = 8.8 Hz, 2.4 Hz, 1H), 7.80 (d, *J* = 8.4 Hz, 2H), 7.69 (d, *J* = 8.0 Hz, 1H), 7.60 (d, *J* = 8.0 Hz, 2H), 3.92 – 3.81 (m, 4H), 2.96 – 2.85 (m, 1H), 2.47 – 2.25 (m, 4H).

1-(2-(3'-Methoxy-2-(trifluoromethyl)-[1,1'-biphenyl]-4-yl)benzo[*d*]oxazol-5-yl)piperidine-4-carboxylic acid (18e). Following general experimental procedure E: Ester **17e** (92 mg, 0.18 mmol), 0.9 mL THF, and 0.2 mL H_2O. LiOH (8.6 mg, 0.36 mmol) were combined to give an off-white solid (72 mg, 81% yield). ^{1}H NMR (400 MHz, MeOD-d4) δ = 8.62 (s, 1H), 8.47 (d, *J* = 8.0 Hz, 1H), 7.91 (s, 1H), 7.85 (d, *J* = 8.4 Hz, 1H), 7.65 – 7.56 (m, 2H), 7.37 (t, *J* = 8.0 Hz, 1H), 7.02 (dd, *J* = 8.4 Hz, 2.8 Hz, 1H), 6.95 – 6.89 (m, 2H), 3.83 (s, 3H), 3.84 – 3.73 (m, 2H), 3.58 – 3.43 (m, 2H), 2.76 (br s, 1H), 2.35 – 2.25 (m, 2H), 2.21 – 2.16 (m, 2H).

***N*-(Cyanomethyl)benzamide (19)**. To an oven-dried 250 mL round-bottom flask equipped with a stirbar was added aminoacetonitrile hydrochloride (8.0 g, 86.5 mmol). Pyridine (50 mL) was carefully added dropwise via addition funnel. Benzoyl chloride (10.5 mL, 90 mmol) was added via addition funnel dropwise over 30 min, and the reaction was stirred overnight (20 h). 70 mL of H_2O added to dissolve the pyridinium hydrochloride and precipitate the product. The new precipitate was filtered, washed with H_2O, dried, and recrystallized from 95% ethanol to give a white crystalline solid (9.5 g, 69% yield). ^{1}H NMR (400 MHz, DMSO-d6) δ = 9.22 (t, *J* = 5.2 Hz, 1H), 7.86 (dd, *J* = 8.0 Hz, 0.8 Hz, 2H), 7.58 (tt, *J* = 7.2 Hz, 1.2 Hz, 1H), 7.50 (t, *J* = 7.6 Hz, 2H), 4.31 (d, *J* = 5.6 Hz, 2H).

***N*-((1*H*-Tetrazol-5-yl)methyl)benzamide (20)**. To a 100 mL round-bottom flask equipped with a stirbar was added nitrile **19** (5.9 g, 36.8 mmol), 32 mL DMF, sodium azide (2.51 g, 38.7 mmol) and ammonium chloride (2.17 g, 40.5 mmol). The reaction vessel was lowered into a pre-heated 125°C oil-bath and stirred overnight (18h). The reaction was cooled to r.t., diluted with 85 mL 2M $HCl_{(aq)}$ causing the product to precipitate. The precipitate was filtered, washed with copious amounts of H_2O and air dried to give a white fluffy solid (6.89 g, 92% yield). ^{1}H NMR (400 MHz, DMSO-d6) δ = 9.27 (t, *J* = 5.6 Hz, 1H), 7.89 (dd, *J* = 8.4 Hz, 1.2 Hz, 2H), 7.57 (tt, *J* = 7.2 Hz, 2.4 Hz, 1H), 7.49 (t, *J* = 7.2 Hz, 2H), 4.76 (d, *J* = 5.6 Hz, 2H).

(1*H*-Tetrazol-5-yl)methanamine hydrochloride (21). To a 250 mL round-bottom flask equipped with a stirbar was added amide **20** (6.89 g, 33.9 mmol) and 50.6 mL 12M $HCl_{(aq)}$. The reaction was equipped with a reflux condenser, placed in a pre-heated 110 °C oil-bath, and stirred at reflux overnight (18 h). The reaction was cooled to r.t., then to 0 °C causing the formation of a precipitate. The reaction mixture was filtered and the filtrate was washed with Et_2O (×2), and concentrated *in vacuo* to give a white solid. This solid was triturated with ethanol and dried under vacuum to give a pale yellow solid (3.59 g, 78% yield). ^{1}H NMR (400 MHz, D_2O) δ = 4.59 (s, 2H).

Methyl 4-(2-fluoroethoxy)benzoate (23). To a 500 mL round-bottom flask equipped with a stirbar was added methyl 4-hydroxybenzoate (**22**) (5.0 g, 32.9 mmol), potassium carbonate (13.6 g, 98.6 mmol), and 219 mL acetone. The reaction vessel was heated to reflux in a pre-heated 70 °C oil-bath, and stirred for 30 min. 1-Bromo-2-fluoroethane (7.34 mL, 98.6 mmol) was added via syringe, and the reaction mixture was stirred for 20 h. The reaction mixture was cooled to r.t. and concentrated *in vacuo*. The resulting solid was dissolved in EtOAc and H_2O. The layers were separated and the aqueous layer was extracted with EtOAc (×1). The combined organic layers were washed with brine, dried over $MgSO_4$, and concentrated *in vacuo* to give a white solid (6.25 g, 96% yield). ^{1}H NMR (400 MHz, $CDCl_3$) δ = 8.00 (d, *J* = 8.8 Hz, 2H), 6.94 (d, *J* = 9.2 Hz, 2H), 4.78 (ddd, *J* = 47.2 Hz, 5.6 Hz, 4.0 Hz, 2H), 4.27 (ddd, *J* = 27.6 Hz, 5.6 Hz, 4.4 Hz, 2H), 3.89 (s, 3H).

4-(2-Fluoroethoxy)benzoic acid (24). To a 500 mL round-bottom flask equipped with a stirbar was added ester **23** (5.84 g, 29.5 mmol), followed by 98 mL methanol and 49 mL H_2O. NaOH (4.71 g, 118 mmol) was added and the reaction mixture was stirred for 16 h at r.t. The reaction was acidified with conc. $HCl_{(aq)}$ to pH = 1 and diluted with H_2O. The resulting precipitate was filtered, washed with H_2O and hexanes, and air-dried to give a white solid (5.41 g, 99%). ^{1}H NMR (400 MHz, $CDCl_3$) δ = 8.05 (d, *J* = 9.2 Hz, 2H), 6.97 (d, *J* = 8.8 Hz, 2H), 4.86 – 4.72 (m, 2H), 4.34 – 4.23 (m, 2H).

N'-Hydroxy-4-(hydroxymethyl)benzimidamide (25).[33] To a 500 mL round-bottom flask equipped with a stirbar was added 4-(hydroxymethyl)benzonitrile (13.3 g, 100 mmol), hydroxyamine hydrochloride (11.1 g, 160 mmol), sodium bicarbonate (26.9 g, 320 mmol), and 167 mL methanol. The reaction was equipped with a reflux condenser and lowered into a pre-heated 70 °C oil-bath. The reaction mixture was stirred for 5 h and then cooled to r.t. The precipitate was filtered and washed with methanol. The filtrate was concentrated *in vacuo* to give a white solid (16.5 g, 99% yield). ^{1}H NMR (400 MHz, MeOD-d_4) matches literature values.

(4-(5-(4-Ethoxyphenyl)-1,2,4-oxadiazol-3-yl)phenyl)methanol (26a).[33] Following general experimental procedure F: 4-Ethoxybenzoic acid (2.49 g, 15.0 mmol), EDC·HCl (2.88 g, 15.0 mmol), HOBt (2.03 g, 15.0 mmol), 19 mL DMF, and

amidine **25** (2.49 g, 15.0 mmol were combined to give an off-white solid (2.2 g, 50% yield). ^{1}H NMR (400 MHz, $CDCl_3$) δ = 8.18 – 8.11 (m, 4H), 7.50 (d, *J* = 8.0 Hz, 2H), 7.02 (d, *J* = 8.8 Hz, 2H), 4.79 (s, 2H), 4.13 (q, *J* = 7.2 Hz, 2H), 1.47 (t, *J* = 6.8 Hz, 3H).

(4-(5-(4-(2-Fluoroethoxy)phenyl)-1,2,4-oxadiazol-3-yl)phenyl)methanol (26b). Following general experimental procedure F: Carboxcyclic acid **24** (2.76 g, 15.0 mmol), EDC·HCl (2.88 g, 15.0 mmol), HOBt (2.03 g, 15.0 mmol), 19 mL DMF, and amidine **25** (2.49 g, 15.0 mmol) were combined to provide the crude product, which was used without further purification for the next step.

(4-(5-(4-(2-Fluoroethoxy)-3-(trifluoromethyl)phenyl)-1,2,4-oxadiazol-3-yl)phenyl)methanol (26c) Following general experimental procedure F: Acid **7a** (3.78 g, 15.0 mmol), EDC•HCl (2.88 g, 15.0 mmol), HOBt (2.54 g, 15.0 mmol), 19 mL DMF, and amidine **25** (2.49 g, 15.0 mmol) were combined to give an off-white solid (3.12 g, 55% yield). ^{1}H NMR (400 MHz, $CDCl_3$) δ = 8.45 (d, *J* = 2.0 Hz, 1H), 8.33 (dd, *J* = 8.8 Hz, 2.0 Hz, 1H), 8.13 (d, *J* = 8.0 Hz, 2H), 7.50 (d, *J* = 8.0 Hz, 2H), 7.16 (d, *J* = 8.4 Hz, 1H), 4.90 – 4.74 (m, 4H), 4.48 – 4.35 (m, 2H) ^{13}C NMR (101 MHz, $CDCl_3$) δ = 174.4, 168.9, 159.7, 144.4, 133.4, 127.8, 127.8 (q, $J_{C\text{-}F}$ = 5.2 Hz), 127.3, 122.9, (q, $J_{C\text{-}F}$ = 274 Hz), 120.4 (q, $J_{C\text{-}F}$ = 32.1 Hz), 117.2, 113.5, 81.4 (d, $J_{C\text{-}F}$ = 173 Hz), 68.5 (d, $J_{C\text{-}F}$ = 21.1 Hz), 64.9 MP: 146-147 °C HRMS (ESI) calcd for $C_{10}H_{14}F_4N_2O_3$ [M+H$^+$] 383.1013. Found [M+H$^+$] 383.1011.

(4-(5-(4-Methoxy-3-(trifluoromethyl)phenyl)-1,2,4-oxadiazol-3-yl)phenyl)methanol (26d). To a 100 ml round-bottom flask equipped with a stirbar was added 4-methoxy-3-(trifluoromethyl)benzoic acid (2.2 g, 10.0 mmol), HOBt (0.39 g, 2.0 mmol), TBTU (3.21 g, 10.0 mmol), 20 ml DMF, and DIPEA (5.23 ml, 30.0 mmol). The reaction was stirred at r.t. for 30 min, and N'-hydroxy-4-(hydroxymethyl)benzimidamide (1.66 g, 10.0 mmol) was added. The reaction was stirred at r.t. for 1 h, heated in a 120 °C oil-bath for 3 h, and cooled to r.t. The reaction mixture was diluted with EtOAc and water. The layers were separated, and the aqueous layer was extracted with EtOAc (×1). The combined organic layers were washed with 1M $HCl_{(aq)}$, water, sat. $NaHCO_{3(aq)}$, water (×3), and brine, dried over $MgSO_4$, and concentrated *in vacuo* to give a tan solid (2.6 g, 74% yield). ^{1}H NMR (400 MHz, $CDCl_3$) δ = 8.45 (d, *J* = 2.0 Hz, 1H), 8.35 (dd, *J* = 8.8 Hz, 2.0 Hz, 1H), 8.15 (d, *J* = 8.0 Hz, 2H), 7.51 (d, *J* = 8.0 Hz, 2H), 7.16 (d, *J* = 8.8 Hz, 1H), 4.80 (s, 2H), 4.02 (s, 3H).

4-(5-(4-Ethoxyphenyl)-1,2,4-oxadiazol-3-yl)benzaldehyde (27a)[33]. To an oven-dried 100 mL round-bottom flask equipped with a stirbar was added 32 mL CH_2Cl_2 and dimethylsulfoxide (1.27 mL, 17.9 mmol). The reaction mixture was cooled in a -78 °C bath ($CO_{2(s)}$ / Acetone). Oxalyl chloride (1.03 mL, 12.1 mmol) was added carefully, and the reaction stirred for 30 min. Alcohol **26a** (1.71 g, 5.77 mmol) was added and the reaction mixture was stirred 30 min. Triethylamine

(6.43 mL, 46.2 mmol) was added and the reaction was allowed to warm to r.t. over 2 h. The reaction mixture was concentrated *in vacuo*, and partitioned between EtOAc & 1M $HCl_{(aq)}$. The layers were separated and the aqueous layer was extracted with EtOAc(×1). The combined organic layers were washed with sat. $NaHCO_{3(aq)}$, water, brine, dried over $MgSO_4$, and concentrated *in vacuo* to give an off-white solid (930 mg, 55% yield). ^{1}H NMR (400 MHz, $CDCl_3$) δ = 10.11 (s, 1H), 8.34 (d, *J* = 8.4 Hz, 2H), 8.15 (d, *J* = 8.8 Hz, 2H), 8.02 (d, *J* = 8.4 Hz, 2H), 7.03 (d, *J* = 8.8 Hz, 2H), 4.14 (q, *J* = 6.8 Hz, 2H), 1.47 (t, *J* = 7.2 Hz, 3H).

4-(5-(4-(2-Fluoroethoxy)phenyl)-1,2,4-oxadiazol-3-yl)benzaldehyde (27b). To an oven-dried 250 mL round-bottom flask equipped with a stirbar was added 53 mL CH_2Cl_2 and dimethylsulfoxide (2.1 mL, 29.6 mmol). The reaction mixture was cooled in a -78 °C bath ($CO_{2(s)}$ / Acetone). Oxalyl chloride (1.7 mL, 20.0 mmol) was added carefully, reaction stirred 30 min. Alcohol **26b** (3.00 g, 9.54 mmol) was added and the reaction mixture was stirred 30 min. Triethylamine (10.6 mL, 76.3 mmol) was added and the reaction was allowed to warm to r.t. over 2 h. The reaction mixture was concentrated *in vacuo*, and partitioned between EtOAc and 1M $HCl_{(aq)}$. The layers were separated and the aqueous layer was extracted with EtOAc(×1). The combined organic layers were washed with sat. $NaHCO_{3(aq)}$, water, brine, dried over $MgSO_4$, and concentrated *in vacuo* to give an off-white solid (1.31 g, 44% yield). ^{1}H NMR (400 MHz, $CDCl_3$) δ = 10.11 (s, 1H), 8.34 (d, *J* = 8.4 Hz, 2H), 8.18 (d, *J* = 9.2 Hz, 2H), 8.02 (d, *J* = 8.4 Hz, 2H), 7.09 (d, *J* = 8.8 Hz, 2H), 4.89 – 4.70 (m, 2H), 4.38 – 4.25 (m, 2H).

4-(5-(4-(2-Fluoroethoxy)-3-(trifluoromethyl)phenyl)-1,2,4-oxadiazol-3-yl)benzaldehyde (27c) To an oven-dried 100 ml round-bottom flask equipped with a stirbar was added 29 mL CH_2Cl_2 and DMSO (1.15 mL, 16.2 mmol). The reaction mixture was cooled to – 78 °C (acetone / $CO_{2(s)}$) and oxalyl chloride (0.93 mL, 11.0 mmol) was added carefully. The reaction mixture was stirred for 30 min at which time alcohol **26c** (2.0 g, 5.23 mmol) was added. The reaction mixture was stirred for 30 min at which time Et_3N (5.83 mL, 41.8 mmol) was added. The cooling bath was removed and the reaction was allowed to warm to r.t. over 2 h. The reaction mixture was concentrated *in vacuo* and partitioned between EtOAc and 1M $HCl_{(aq)}$. The layers were separated and the aqueous layer was extracted with EtOAc (×2). The combined organic layers were washed with 1M $HCl_{(aq)}$, sat. $NaHCO_{3(aq)}$, brine, dried over $MgSO_4$, concentrated *in vacuo,* and triturated with MTBE to give a pale-yellow solid (1.75 g, 88% yield). ^{1}H NMR (400 MHz, $CDCl_3$) δ = 10.11 (s, 1H), 8.47 (d, *J* = 1.6 Hz, 1H), 8.39 – 8.31 (m, 3H), 8.02 (d, *J* = 8.4 Hz, 2H), 7.19 (d, *J* = 8.8 Hz, 1H), 4.93 – 4.75 (m 2H), 4.49 – 4.35 (m, 2H) ^{13}C NMR (101 MHz, $CDCl_3$) δ = 191.7, 174.9, 168.3, 159.9, 138.2, 133.5, 132.2, 130.2, 128.3, 127.9 (q, $J_{C\text{-}F}$

= 5.4 Hz), 122.9 (q, J_{C-F} = 274 Hz), 120.5 (q, J_{C-F} = 32.3 Hz), 116.9, 113.6, 81.4 (d, J_{C-F} = 173 Hz), 68.6 (d, J_{C-F} = 21.1 Hz) MP: 149-150 °C HRMS (ESI) calcd for $C_{18}H_{13}F_4N_2O_3$ [M+H$^+$] 381.0857. Found [M+H$^+$] 381.0857.

4-(5-(4-Methoxy-3-(trifluoromethyl)phenyl)-1,2,4-oxadiazol-3-yl)benzaldehyde (27d). To an oven-dried 100 ml round-bottom flask equipped with a stirbar was added 32 mL CH_2Cl_2 and DMSO (1.26 mL, 17.7 mmol). The reaction mixture was cooled to – 78 °C (acetone / $CO_{2(s)}$) and oxalyl chloride (1.01 mL, 12.0 mmol) was added carefully. The reaction mixture was stirred for 30 min at which time alcohol **26d** (2.0 g, 5.71 mmol) was added. The reaction mixture was stirred for 30 min at which time Et_3N (6.37 mL, 45.7 mmol) was added. The cooling bath was removed and the reaction was allowed to warm to r.t. over 2 h. The reaction mixture was concentrated *in vacuo* and partitioned between EtOAc and 1M $HCl_{(aq)}$. The layers were separated and the aqueous layer was extracted with EtOAc (×2). The combined organic layers were washed with 1M $HCl_{(aq)}$, sat. $NaHCO_{3(aq)}$, brine, dried over $MgSO_4$, and concentrated *in vacuo* to give a pale-yellow solid (1.51 g, 76% yield). ^{1}H NMR (400 MHz, $CDCl_3$) δ = 10.11 (s, 1H), 8.46 (s, 1H), 8.40 – 8.32 (m, 3H), 8.03 (d, *J* = 8.0 Hz, 2H), 7.19 (d, *J* = 8.8 Hz, 1H), 4.04 (s, 3H).

1-(4-(5-(4-Ethoxyphenyl)-1,2,4-oxadiazol-3-yl)benzyl)azetidine-3-carboxylic acid (28a).[33] Following general experimental procedure G: Aldehyde **27a** (500 mg, 1.70 mmol), azetidine-3-carboxylic acid (180 mg, 1.79 mmol), 24 mL methanol, 0.85 mL acetic acid, and $NaBH_3CN$ (53 mg, 0.85 mmol) in 3.4 mL were combined to give a white solid (331 mg, 51% yield). ^{1}H NMR (400 MHz, DMSO-d6) δ = 8.11 (d, *J* = 8.8 Hz, 2H), 8.01 (d, *J* = 8.0 Hz, 2H), 7.47 (d, *J* = 8.4 Hz, 2H), 7.17 (d, *J* = 8.8 Hz, 2H), 4.16 (q, *J* = 7.2 Hz, 2H), 3.64 (s, 2H), 3.45 – 3.38 (m, 1H), 3.28 – 3.15 (m, 4H), 1.37 (t, *J* = 6.8 Hz, 3H).

1-(4-(5-(4-(2-Fluoroethoxy)phenyl)-1,2,4-oxadiazol-3-yl)benzyl)azetidine-3-carboxylic acid (28b). Following general experimental procedure G: Aldehyde **27b** (500 mg, 1.60 mmol), azetidine-3-carboxylic acid (170 mg, 1.68 mmol),23 mL methanol, 0.8 mL acetic acid, and $NaBH_3CN$ (50 mg, 0.80 mmol) in 3.2 mL methanol were combined to give 400 mg of 85% pure acetate salt ^{1}H NMR. ^{1}H NMR (400 MHz, MeOD-d4) δ = 8.21 (d, *J* = 8.0 Hz, 2H), 8.18 (d, *J* = 8.8 Hz, 2H), 7.62 (d, *J* = 8.0 Hz, 2H), 7.19 (d, *J* = 8.8 Hz, 2H), 4.85 – 4.69 (m, 2H), 4.42 – 4.30 (m, 2H), 4.37 (s, 2H), 4.19 – 4.09 (m, 4H), 3.41 (pent, *J* = 8.4 Hz, 1H), 1.96 (s, 3H).

1-(4-(5-(4-(2-Fluoroethoxy)-3-(trifluoromethyl)phenyl)-1,2,4-oxadiazol-3-yl)benzyl)azetidine-3-carboxylic acid (28c) Following general experimental procedure G: Aldehyde **27c** (500 mg, 1.31 mmol), azetidine-3-carboxylic acid (139 mg, 1.38 mmol), 19 mL MeOH, 0.70 mL AcOH, and $NaBH_3CN$ (41 mg, 0.70 mmol) in 2.6 mL MeOH were combined to give an off-white solid (317 mg, 52% yield). ^{1}H NMR (400 MHz, MeOD-d4) δ = 8.45 – 8.38 (m, 2H), 8.23 (d, *J* = 8.0 Hz,

2H), 7.64 (d, J = 8.0 Hz, 2H), 7.46 (d, J = 9.6 Hz, 1H), 4.87 – 4.71 (m, 2H), 4.54 – 4.43 (m, 2H), 4.43 (s, 2H), 4.25 – 4.15 (m, 4H), 3.44 (pent, J = 8.8 Hz, 1H) ^{13}C NMR (101 MHz, MeOD-d4) δ = 166.3, 160.5, 151.8, 137.2, 125.3, 119.0, 118.8, 118.7, 118.6 (q, J_{C-F} = 5.45 Hz), 117.3, 114.9 (q, J_{C-F} = 273 Hz), 111.3 (q, J_{C-F} = 32.0 Hz), 108.4, 105.8, 105.8, 73.1 (d, J_{C-F} = 70.4 Hz), 60.7, 60.5, 55.2 (d, J_{C-F} = 11.0 Hz), 55.1 MP: 146-148 °C Anal. Calcd for $C_{22}H_{19}F_4N_3O_4$•$2H_2O$: C, 52.70; H, 4.62; N, 8.38. Found: C, 52.93; H, 4.46; N, 8.37 HRMS (ESI) calcd for $C_{22}H_{20}F_4N_3O_4$ [M+H$^+$] 466.1384. Found [M+H$^+$] 466.1383.

1-(4-(5-(4-(2-Fluoroethoxy)-3-(trifluoromethyl)phenyl)-1,2,4-oxadiazol-3-yl)benzyl)piperidine-4-carboxylic acid (28d). Following general experimental procedure G: Aldehyde **27c** (380 mg, 1.0 mmol), piperidine-4-carboxylic acid (136 mg, 1.05 mmol), 14.3 mL MeOH, 0.5 mL AcOH, and $NaBH_3CN$ (31 mg, 0.5 mmol) in 2 mL methanol were combined to give a white solid (193 mg, 39% yield). ^{1}H NMR (400 MHz, DMSO-d6) δ = 8.45 (dd, J = 8.8 Hz, 1.6 Hz, 1H), 8.33 (d, J = 1.6 Hz, 1H), 8.05 (d, J = 8.0 Hz, 2H), 7.58 (d, J = 8.8 Hz, 1H), 7.51 (d, J = 8.0 Hz, 2H), 4.75 – 4.50 (m, 4H), 3.54 (s, 2H), 3.25 – 1.51 (m, 9H).

***N*-((1*H*-Tetrazol-5-yl)methyl)-1-(4-(5-(4-(2-fluoroethoxy)-3-(trifluoromethyl)phenyl)-1,2,4-oxadiazol-3-yl)phenyl)methanamine (28e)**. Following general experimental procedure G: Aldehyde **27c** (380 mg, 1.0 mmol), **21** (142 mg, 1.05 mmol), 14.3 mL MeOH, 0.5 mL AcOH, and $NaBH_3CN$ (31 mg, 0.5 mmol) in 2 mL methanol were combined. The reaction mixture was stirred for 3 h, diluted with MTBE to give a precipitate. The precipitate was filtered to give an off-white solid (145 mg, 31% yield). ^{1}H NMR (400 MHz, MeOD-d4) δ = 8.46 – 8.42 (m, 2H), 8.24 (d, J = 8.4 Hz, 2H), 7.70 (d, J = 8.0 Hz, 2H), 7.48 (d, J = 8.4 Hz, 1H), 4.83 – 4.72 (m, 2H), 4.54 – 4.44 (m, 2H), 4.50 (s, 2H), 4.40 (s, 2H).

1-(4-(5-(4-Methoxy-3-(trifluoromethyl)phenyl)-1,2,4-oxadiazol-3-yl)benzyl)azetidine-3-carboxylic acid (28f). Following general experimental procedure G: Aldehyde **27d** (500 mg, 1.44 mmol), azetidine-3-carboxylic acid (152 mg, 1.51 mmol), 21 mL methanol, 0.72 mL acetic acid, and $NaBH_3CN$ (45 mg, 0.72 mmol) in 2.9 mL methanol were combined to give a white solid (300 mg, 48% yield). ^{1}H NMR (400 MHz, DMSO-d6) δ = 8.43 (d, J = 8.4 Hz, 1H), 8.30 (s, 1H), 8.02 (d, J = 7.2 Hz, 2H), 7.60 – 7.42 (m, 3H), 4.03 (s, 3H), 3.64 (br s, 2H), 3.23 (br s, 3H).

4-(3-(4-(Hydroxymethyl)phenyl)-1,2,4-oxadiazol-5-yl)-2-(trifluoromethyl)phenol (30) To a 100 ml round-bottom flask equipped with a stirbar was added 4-hydroxy-3-(trifluoromethyl)benzoic acid (**29**) (2.06 g, 10.0 mmol), HOBt (0.39 g, 2.0 mmol), TBTU (3.21 g, 10.0 mmol), 20 ml DMF, and DIPEA (5.23 ml, 30.0 mmol). The reaction was stirred at r.t. for 30 min, and **25** (1.66 g, 10.0 mmol) was added. The reaction was stirred at r.t. for 1 h, heated in a 120 °C oil-bath for 3 h, and cooled to r.t. The reaction mixture was diluted with EtOAc and water. The layers were separated, and the aqueous layer

was extracted with EtOAc (×1). The combined organic layers were washed with 1M $HCl_{(aq)}$, water, sat. $NaHCO_{3(aq)}$, water (×3), and brine, dried over $MgSO_4$, and concentrated *in vacuo* to give a tan solid (1.7 g, 51% yield). ^{1}H NMR (400 MHz, DMSO-d6) δ = 11.83 (br s, 1H), 8.29 – 8.22 (m, 2H), 8.04 (d, *J* = 8.0 Hz, 2H), 7.52 (d, *J* = 8.0 Hz, 2H), 7.27 (d, *J* = 8.4 Hz, 1H), 5.38 (br s, 1H), 4.60 (s, 2H) ^{13}C NMR (101 MHz, DMSO-d6) δ = 174.3, 168.1, 160.0, 146.4, 133.5, 126.9, 126.8 (q, J_{C-F} = 5.6 Hz), 124.5, 123.3 (q, J_{C-F} = 274 Hz), 118.2, 118.1, 116.4 (q, J_{C-F} = 31.0 Hz), 114.0, 62.5 MP: > 200 °C HRMS (ESI, m/z) calcd for $C_{16}H_{11}F_3N_2O_3$ [M+H$^+$] 337.0795. Found [M+H$^+$] 337.0789.

4-(5-(4-Hydroxy-3-(trifluoromethyl)phenyl)-1,2,4-oxadiazol-3-yl)benzaldehyde (31) To a 250 mL round-bottom flask equipped with a stirbar was added alcohol **30** (1.0 g, 2.97 mmol), 59 mL 1,4-dioxane, and 10 g MnO_2. A reflux condenser was added then the reaction was heated in an 80 °C oil-bath and stirred 4 h at which point TLC showed consumption of the alcohol. The reaction mixture was cooled to r.t. and filtered through a Celite plug, washing with EtOAc. The filtrate was concentrated *in vacuo* to give a tan solid (620 mg, 62% yield). ^{1}H NMR (400 MHz, DMSO-d6) δ = 10.11 (s, 1H), 8.34 – 8.22 (m, 4H), 8.10 (d, *J* = 8.0 Hz, 2H), 7.24 (d, *J* = 8.4 Hz, 1H) ^{13}C NMR (101 MHz, DMSO-d6) δ = 192.7, 174.9, 167.5, 160.7, 138.0, 133.7, 131.2, 130.2, 127.8, 126.9 (q, J_{C-F} = 5.66 Hz), 123.3 (q, J_{C-F} = 274 Hz), 118.3, 116.4 (q, J_{C-F} = 30.8), 113.3, MP: > 200 °C HRMS (ESI, m/z) calcd for $C_{16}H_8F_3N_2O_3$ [M-H] 333.0493. Found [M-H] 333.0400.

Methyl 1-(4-(5-(4-hydroxy-3-(trifluoromethyl)phenyl)-1,2,4-oxadiazol-3-yl)benzyl)azetidine-3-carboxylate (32) To a 25 ml round-bottom flask equipped with a stirbar was added aldehyde **31** (300 mg, 0.90 mmol), 4.1 ml CH_2Cl_2, methyl azetidine-3-carboxylate hydrochloride (204 mg, 1.35 mmol), AcOH (0.21 ml, 3.6 mmol), DIPEA (0.24 ml, 1.35 mmol), and 4.1 ml MeOH. The reaction mixture was stirred for 30 min and sodium cyanoborohydride (57 mg, 0.90 mmol) was added. The reaction mixture was stirred for 2 h at which time TLC showed consumption of the aldehyde. The reaction mixture was concentrated *in vacuo*, dissolved in EtOAc and quenched with sat. $NaHCO_{3(aq)}$. The layers were separated and the aqueous layer was extracted with EtOAc (×2). The combined organic layers were washed with water and brine, dried over $MgSO_4$, and concentrated *in vacuo*. The crude product was purified on a silica gel column eluted with 75 – 100% EtOAc/ hexanes to give a white crystalline solid (193 mg, 49% yield). ^{1}H NMR (400 MHz, MeOD-d4) δ = 8.14 (d, *J* = 1.2 Hz, 1H), 8.00 (d, *J* = 8.8 Hz, 1.6 Hz, 1H), 7.91 (d, *J* = 8.0 Hz, 2H), 7.33 (d, *J* = 8.0 Hz, 2H), 6.95 (d, *J* = 8.8 Hz, 1H), 3.72 – 3.62 (m, 5H), 3.56 (t, *J* = 8.0 Hz, 2H), 3.45 (t, *J* = 6.8 Hz, 2H), 3.34 (pent, *J* = 7.6 Hz, 1H) ^{13}C NMR (101 MHz, MeOD-d4) δ = 174.8, 173.1, 168.1, 161.4, 139.6, 132.7, 129.0, 127.1, 126.9 (q, J_{C-F} = 5.15 Hz), 126.0, 123.5 (q, J_{C-F} = 273 Hz), 117.8, 117.4 (q, J_{C-F} = 31.1 Hz), 113.5, 61.8, 56.1, 51.2, 33.4 MP: 125 °C (decomposition) HRMS (ESI, m/z) calcd for $C_{22}H_{18}F_3N_3O_4$ [M+H$^+$] 434.1322. Found [M+H$^+$] 434.1320.

2-(4-(3-(4-Formylphenyl)-1,2,4-oxadiazol-5-yl)-2-(trifluoromethyl)phenoxy)ethyl 4-methylbenzenesulfonate (33) To a 50 mL round-bottom flask equipped with a stirbar was added phenol **31** (450 mg, 1.35 mmol), ethylene 1,2-bis(tosylate) (748 mg, 2.02 mmol), potassium carbonate (933 mg, 6.75 mmol), and 6.8 mL acetonitrile. The reaction vessel was equipped with a reflux condenser placed in a pre-heated 90 °C oil-bath. The reaction mixture was stirred overnight (~18 h), cooled to r.t., and diluted with EtOAc & water. The layers were separated, and the aqueous layer was extracted with EtOAc (×3). The combined organic layers were washed with brine, dried over $MgSO_4$, and concentrated *in vacuo*. The product was purified by silica-gel chromatography to give an off-white solid (210 mg, 29% yield). ^{1}H NMR (400 MHz, $CDCl_3$) δ = 10.07 (s, 1H), 8.37 (d, *J* = 1.6 Hz), 8.34 – 8.24 (m, 3H), 7.98 (d, *J* = 8.4 Hz, 2H), 7.79 (d, *J* = 8.4 Hz, 2H), 7.33 (d, *J* = 8.4 Hz, 2H), 7.09 (d, *J* = 8.8 Hz, 1H), 4.46 – 4.33 (m 4H), 2.43 (s, 3H), ^{13}C NMR (100 MHz, $CDCl_3$) δ = 191.7, 174.7, 168.2, 159.4, 145.3, 138.2, 133.5, 132.4, 132.1, 130.1, 130.0, 128.2, 128.0, 127.7 (q, $J_{C\text{-}F}$ = 5.35 Hz), 122.7, (q, $J_{C\text{-}F}$ = 274 Hz), 120.2, (q, $J_{C\text{-}F}$ = 32.1 Hz), 116.9, 113.5, 67.4, 66.7, 21.7, MP: 125 °C (decomposition) HRMS (ESI, m/z) calcd for $C_{25}H_{20}F_3N_2O_6S$ [M+H$^+$] 533.0989. Found [M+H$^+$] 533.0990.

Methyl 1-(4-(5-(4-(2-(tosyloxy)ethoxy)-3-(trifluoromethyl)phenyl)-1,2,4-oxadiazol-3-yl)benzyl)azetidine-3-carboxylate (34) To a 25 mL round-bottom flask equipped with a stirbar was added aldehyde **33** (200 mg, 0.38 mmol), methyl 3-azetidinecarboxylate hydrochloride (61 mg, 0.40 mmol), 1.9 mL 1,2-dichloroethane, and 6.3 mL methanol. Diisopropylethylamine (0.07 mL, 0.41 mmol) was added to the reaction mixture, and it was stirred for 1 h at r.t. The reaction mixture was concentrated *in vacuo*, suspended in 1.9 mL 1,2-dichloroethane, at which time sodium triacetoxyborohydride (250 mg, 1.18 mmol) and acetic acid (0.02 mL, 0.38 mmol) were added. The reaction mixture was stirred overnight (~18 h), diluted with EtOAc, and quenched with sat. $NaHCO_{3(aq)}$. The layers were separated, and the aqueous layer extracted with EtOAc (× 3). The combined organic layers were washed with water and brine, dried over $MgSO_4$, and concentrated *in vacuo*. The crude product was purified on a silica gel column eluted with 2-3 % MeOH/ CH_2Cl_2 to give a clear oil (110 mg, 41% yield). ^{1}H NMR (400 MHz, $CDCl_3$) δ = 8.40 (s, 1H), 8.29 (d, *J* = 8.8 Hz, 1H), 8.08 (d, *J* = 6.8 Hz, 2H), 7.79 (d, *J* = 7.2 Hz), 7.41 (d, *J* = 5.6 Hz, 2H), 7.33 (d, *J* = 5.6 Hz, 2H), 7.07 (dd, *J* = 8.4 Hz, 2.4 Hz, 1H), 4.45 – 4.32 (m 4H), 3.74 – 3.64 (m, 5H), 3.60 – 3.50 (m, 2H), 3.42 – 3.28 (m, 3H), 2.45 – 2.38 (m, 3H), ^{13}C NMR (100 MHz, $CDCl_3$) δ = 174.1, 173.5, 168.8, 159.0, 145.2, 141.2, 133.3, 132.3, 129.9, 128.9, 127.9, 127.6 (q, $J_{C\text{-}F}$ = 5.35 Hz), 127.6, 125.5, 122.6, (q, $J_{C\text{-}F}$ = 274 Hz), 119.7 (q, $J_{C\text{-}F}$ = 32.2 Hz), 117.2, 113.2, 67.2, 66.5, 63.1, 56.9, 52.0, 33.9, 21.6; HRMS (ESI, m/z) calcd for $C_{30}H_{29}F_3N_3O_7S$ [M+H$^+$] 632.1673. Found [M+H$^+$] 632.1669.

4.2 *In vitro* screening

4.2.1 *In vitro* functional assay (EC_{50})

The functional assay of the test compounds was carried out according to published procedure.[51] Briefly, $S1P_1$-TANGO-U2OS cells were suspended at a concentration of 312,500 cells/mL in assay medium (Freestyle Expression Medium without supplements). 32 µL of the cell suspension was seeded in each well of a black, clear-bottom 384-well plates, followed by 48 h incubation at 37 °C in 5% CO_2 and 95% relative humidity. After incubation, 100 nL of the test compound in DMSO was added to sample wells, while DMSO alone (0.5 % final concentration) was added to control wells. Plates were then incubated at 37 °C in 5% CO_2 for 5 h. After incubation, 8 µL/well of the LiveBLAzer FRET substrate mixture, prepared according to the manufacturer's protocol and containing 10 mM Probenicid, was added to all wells. After 2 h incubation at r.t. in the dark, plates were read on the EnVision plate reader (PerkinElmer Lifesciences, Turku, Finland) at an excitation wavelength of 405 nm and emission wavelengths of 460 nm and 535 nm.

4.2.2 *In vitro* binding assay (IC_{50})

The potency of the test compounds for S1P receptors was determined according to our published procedure.[34] In brief, test compounds dissolved in DMSO were pre-incubated for 30 min at r.t. in assay buffer (50 mM HEPES-Na (pH 7.5), 5 mM $MgCl_2$, 1 mM $CaCl_2$, 0.5% fatty acid-free BSA) with cell membranes expressing recombinant human $S1P_{1-3}$ ($S1P_1$ cell membranes were purchased from ChanTest Corp, Cleveland, OH, $S1P_2$ and $S1P_3$ cell membranes were from Chemicon/Millipore Inc., Billerica, MA). Diluted [^{32}P]S1P, prepared in-house, was added to give a final volume of 150 µL containing 0.1-0.2 nM [^{32}P]S1P with 1-2 µg membrane protein in each well of a 96-well plate. Samples were incubated for 60 min at r.t. and filter-bound radioactivity was measured by Cherenkov counting on a Beckman LS 3801 scintillation counter. Non-specific binding was determined from samples incubated with an additional 1 µM cold S1P.

4.3 Radiochemistry

[^{18}F]Fluoride was produced by $^{18}O(p,n)^{18}F$ reaction through proton irradiation of enriched ^{18}O water (95%) using Washington University's RDS111 cyclotron (Siemens/CTI Molecular Imaging, Knoxville, TN). [^{18}F]Fluoride was firstly passed through an ion-exchange resin and then eluted with 0.02 M potassium carbonate (K_2CO_3) solution. A sample of ~200 mCi [^{18}F]/fluoride was added to a reaction vessel containing Kryptofix 222 (5-6 mg), and the solution was evaporated under nitrogen (oil-bath temperature 110 °C). Acetonitrile (3 × 1.0 mL) was added and evaporated to ensure complete removal of water. After all of the water was removed, 1 mg of **34** was added as a solution in 200 µL acetonitrile. The reaction tube was capped, briefly mixed, and placed in a pre-heated 110 °C oil-bath. The reaction mixture was incubated at 110 °C for 15 min, shaking occasionally. The reaction vessel was removed from the oil-bath, at which time

300 μL EtOH and 200 μL $NaOH_{(aq)}$ were added. The reaction mixture was heated in an 80 °C pre-heated oil-bath for 5 min, shaking occasionally. The reaction vessel was removed from the oil-bath, quenched with 400 μL 1M $HCl_{(aq)}$ and diluted with 1.9 mL of the HPLC mobile phase (38% MeCN in 0.1 M ammonium formate buffer, pH = 4.5), passed through an alumina Neutral Sep-Pak Plus cartridge. The crude product was then loaded onto an Agilent SB-C18 semi-preparative HPLC column (250 mm × 10 mm) with a UV detector set at 254 nm. The HPLC system used a 5 mL injection loop. With the above mentioned mobile phase at 4.0 mL/min flow rate. The retention time of the product was approximately 18 min. After the HPLC collection was diluted with ~50 mL sterile water, the product was trapped on a C18 Sep-Pak Plus cartridge. The trapped product was eluted with ethanol (0.3 mL), and this portion was discarded. The Sep-Pak was sequentially eluted with ethanol (0.3 mL) which was followed by 2.7 mL of 0.9% saline. After sterile filtration into a glass vial, the final product was ready for quality control (QC) analysis and animal studies. An aliquot of sample was assayed by an analytical HPLC system (Agilent Zorbax, SB-C18 column, 250 × 4.6 mm), UV at 254 nm; mobile phase consists of acetonitrile/0.1 M, pH 4.5 ammonium formate buffer (50/50, v/v). At this condition, the retention time for [^{18}F]**28c** was approximately 5.1 min at a flow rate of 1.0 mL/min. The radioactive dose was authenticated by co-injection with the corresponding nonradioactive compound **28c** onto an analytical HPLC system. The radiochemical purity was > 98%, the labeling yield was 25.7 ± 4.6% (n = 10, decay corrected to start of synthesis) and the specific activity was 1.43 ± 0.12 Ci/μmol (decay corrected to the end of synthesis). The entire procedure took about 90 min.

4.4 Biological evaluation in rodents

All animal experiments were conducted under Washington University Animal Studies Committee IACUC-approved protocols in accordance with the US National Research Council's Guide for the Care and Use of Laboratory Animals. Adult male Sprague Dawley rats (Charles River Inc.) were used to determine the biodistribution in normal rodents. Adult male C57BL/6 mice (Charles River Inc., Frederick, MD) were used for the mouse model of LPS-induced liver injury and inflammation to demonstrate specificity of the $S1P_1$ tracer.[50, 52-54] LPS-treated mice received an intraperitoneal injection of LPS from E. coli 055:B5 (Sigma-Aldrich, St. Louis, MO, USA) in saline (3 mg/mL) at 15 mg/kg (5 mL/kg) dose 24 hours prior to use, sham mice received a saline injection.

4.4.1 Biodistribution in normal rats.

The biodistribution of [^{18}F]**28c** in normal rodents was determined using adult male SD rats (230-270 g). Rats were anesthetized with isoflurane (2-3% in oxygen) and injected in the tail vein with ~50 μCi (1.85 MBq) of [^{18}F]**28c** in 5% ethanol/saline. At the appropriate time, rats were again anesthetized and were euthanized at 5, 30, 60 and 120 min post-

injection (n = 4 for each group). Tissues of interest including blood, heart, lung, muscle, fat, pancreas, spleen, bone, thymus, brain, kidney, and liver were collected, weighed, and counted with a dilution of the injectate on an automated well counter (Beckman Gamma 8000 well counter). Uptake in Table 3 is reported as decay-corrected percent injected dose per gram (%ID/g).

4.4.2 *In vitro* autoradiography and IHC in LPS-treated mice.

Livers from sham and LPS treated mice were collected and snap frozen. 20 μm sequential sections were cut with a Microm cryotome and thaw mounted on glass slides. The slides were then incubated for 60 min with ~0.1 nM [^{18}F]**28c** at r.t. Blocking studies were performed using adjacent sections incubated with an additional 10 μM of either S1P or SEW2871. Following the incubation, the slides were washed and exposed to the storage phosphor screen in an imaging cassette for 12 h in -80 °C in the dark. The distribution of radioactivity was visualized with a Fuji Bio-Imaging Analyzer FLA-7000 (Fuji Photo Film, Tokyo, Japan).

4.4.3 IHC staining of $S1P_1$ expression in mouse liver.

Liver samples were fixed in 10% formalin immediately, then embedded in paraffin and cut into 5 μm sections. Sections were deparaffinized in xylene and rehydrated through a graded alcohol series to water. Endogenous peroxidase activity was quenched with 3% H_2O_2 in methanol for 5 min. Slides were incubated in blocking buffer (10% normal goat serum in PBS) for 30 min before the incubation with a 1:50 dilution of a rabbit anti-mouse $S1P_1$ antibody (Santa Cruz biotechnology, Santa Cruz, CA) overnight at 4 °C. The primary antibody binding was detected using an anti–rabbit HRP-DAB staining kit (R&D Systems, Minneapolis, MN) according to the manufacturer's instructions. A Nikon E600 microscope coupled with a charge-coupled device camera was used to obtain all photomicrographs.

4.4.4 MicroPET imaging of LPS-treated mice with [^{18}F]28c and [^{15}O]water

MicroPET studies were performed using adult male C57BL/6 mice (18 -23 g) ~24 h after pre-treatment with either saline (n=4) or LPS (n=3), PET scans were conducted under light anesthesia (2-3 % isoflurane) delivered by a nose cone. Mice were secured using a custom-designed acrylic restraining device, and placed in transaxial position with their whole bodies inside the field of the window of the Inveon PET/CT system. Following a transmission scan and a CT for anatomical co-registration, animals received a bolus injection [^{18}F]**28c** (~ 300 μCi (11.1 MBq), in 10% ethanol/saline) was injected i.v. and a microPET dynamic scan acquired from 0 - 120 min.. After reconstruction of the microPET data, the liver ROI was drawn by co-registration with CT images, and the data was analyzed using the Inveon Research Workstation built-in software IRW 4.2 program (Siemens Inc., Erlangen, Germany) to calculate the standard uptake value (SUV).

[^{15}O]Water microPET study. Small-animal microPET imaging using [^{15}O]water serves as a non-invasive method to measure liver blood flow in rodents.[48] A microPET scan was performed ~30 mins before the [^{18}F] scan on an Inveon PET/CT system (Siemens Inc., Erlangen, Germany). Following a transmission scan and a CT for anatomical co-registration, animals received a bolus injection (30 - 55 MBq) of [^{15}O]water via the tail vein, immediately followed by a 10 min scan (1×3 s, 6×2 s, 5×5 s, 11×10 s, 5×30 s, 5×60 s).

MicroPET data processing. Image reconstructions were performed using microPET Manager 2.3.3.6, ASIPro 6.3.3.0 (Siemens Inc., Erlangen, Germany). The list-mode data of the emission scans were reframed into a dynamic sequence. The data was reconstructed per time frame employing an iterative reconstruction algorithm, and corrected for decay, random coincidences, scatter and attenuation. Three-dimensional region of interest (ROI) of mouse liver was drawn according to a standard mouse anatomy atlas. Averaged regional radioactivity was obtained and expressed as dimensionless standardized uptake values (SUVs). The parameter standardized uptake value (SUV) is defined as [tissue activity concentration (MBq/g) × body weight (g)/injected dose (MBq)]. For statistical analysis, two-tail student t test was applied, and significant difference is defined as P value < 0.05.

4.4.5 Biodistribution of [^{18}F]28c and [^{99m}Tc]Mebrofenin in LPS-treated mice.

The acute biodistribution studies in sham and LPS-treated mice, as described above, was carried out to determine tracer uptake in a rodent model with increased $S1P_1$. Approximately 24 hours after treatment, one set of sham and LPS-treated mice was injected in the tail vein with ~20 μCi (0.74 MBq) of [^{18}F]**28c** in 10% ethanol/saline A separate set of sham and LPS-treated mice were injected ~4 μCi (148 KBq) of [^{99m}Tc]mebrofenin (Cardinal Health Nuclear Pharmacy Services, Overland, MO) under 2-3% isoflurane/ oxygen anesthesia. Animals (n=4 per each group for each tracer) were euthanized at 30 or 60 min post-injection. Tissues of interest were collected, weighed, and counted with a dilution of the injectate on an automated well counter (Beckman Gamma 8000 well counter). Uptake is reported as background- and decay-corrected percent injected dose per gram (%ID/g).

ANCILLARY INFORMATION

Supporting Information

Molecular formula strings (CSV) of the final products

AUTHOR INFORMATION

Corresponding Author

*Telephone: 314-362-8487. Fax: 314-262-8555. E-mail: tuz@mir.wustl.edu. Tax: 1-314-362-8555

Notes

The authors declare no competing financial interest.

ACKNOWLEDGMENT

The authors wish to thank Ms. Lynne Jones for her many helpful discussions. This research work was directly supported by the Department of Energy (DOE, No. DESC0008432, and No. DESC0012737), and the National Institutes of Health through the National Institute of Neurological Disorders and Stroke (NINDS, R01NS075527), and the National Institute of Mental Health (NIMH, No. MH092797). During the process of accomplishing this work, it also used the NIH/NIGMS Biomedical Mass Spectrometry Resource at Washington University in St. Louis, MO, which is supported by National Institutes of Health/ National Institute of General Medical Sciences Grant # 8P41GM103422. We are grateful to the Washington University Cyclotron Facility and its personnel for [^{18}F]fluoride production. We thank the Department of Chemistry staff and the Washington University High Resolution NMR Facility for assistance with NMR spectra; purchase of the 400 MHz NMR instrument was partially supported by Grant S10 RR027207 from the NIH Shared Instrument Grant program. We also thank the Elvie L. Taylor Histology Core Facility of Washington University School of Medicine for sample embedding, and the MIR Pre-clinical PET-CT facility of the Washington University School of Medicine, which was funded in part through the National Institute of Health HEI grant (S10 RR025097).

ABBREVIATIONS

%ID/g, percent injected dose per gram; EDC•HCl, *N*-(3-Dimethylaminopropyl)-*N′*-ethylcarbodiimide hydrochloride; ROI, region of interest; SD, standard deviation; S1P, sphingosine 1-phosphate; $S1P_{1\text{-}5,}$ sphingosine 1-phosphate receptor 1-5; SPhos, 2-dicyclohexylphosphino-2',6'-dimethoxybiphenyl; SUV, standardized uptake value; TAC, time-activity curve; [^{99m}Tc]-mebrofenin,' [^{99m}Tc]-*N*-(3-bromo-2,4,6-trimethyacetanilide) iminodiacetic acid; XPhos, 2-Dicyclohexylphosphino-2′,4′,6′-triisopropylbiphenyl.

REFERENCES

(1) O'Sullivan, C.; Dev, K. K. The structure and function of the S1P1 receptor. *Trends Pharmacol. Sci.* **2013**, *34*, 401-412.

(2) Rosen, H.; Germana Sanna, M.; Gonzalez-Cabrera, P. J.; Roberts, E. The organization of the sphingosine 1-phosphate signaling system. In *Sphingosine-1-Phosphate Signaling in Immunology and Infectious*

Diseases, 2014/04/15 ed.; Oldstone, M. B. A., Rosen, H. Eds.; Springer International Publishing, Switzerland, 2014; Vol. 378, pp 1-21.

(3) Billich, A.; Bornancin, F.; Devay, P.; Mechtcheriakova, D.; Urtz, N.; Baumruker, T. Phosphorylation of the immunomodulatory drug FTY720 by sphingosine kinases. *J. Biol. Chem.* **2003**, *278*, 47408-47415.

(4) Mandala, S.; Hajdu, R.; Bergstrom, J.; Quackenbush, E.; Xie, J.; Milligan, J.; Thornton, R.; Shei, G. J.; Card, D.; Keohane, C.; Rosenbach, M.; Hale, J.; Lynch, C. L.; Rupprecht, K.; Parsons, W.; Rosen, H. Alteration of lymphocyte trafficking by sphingosine-1-phosphate receptor agonists. *Science* **2002**, *296*, 346-349.

(5) Brinkmann, V.; Billich, A.; Baumruker, T.; Heining, P.; Schmouder, R.; Francis, G.; Aradhye, S.; Burtin, P. Fingolimod (FTY720): Discovery and development of an oral drug to treat multiple sclerosis. *Nat. Rev. Drug Discovery* **2010**, *9*, 883-897.

(6) Forrest, M.; Sun, S. Y.; Hajdu, R.; Bergstrom, J.; Card, D.; Doherty, G.; Hale, J.; Keohane, C.; Meyers, C.; Milligan, J.; Mills, S.; Nomura, N.; Rosen, H.; Rosenbach, M.; Shei, G. J.; Singer, II; Tian, M.; West, S.; White, V.; Xie, J.; Proia, R. L.; Mandala, S. Immune cell regulation and cardiovascular effects of sphingosine 1-phosphate receptor agonists in rodents are mediated via distinct receptor subtypes. *J. Pharmacol. Exp. Ther.* **2004**, *309*, 758-768.

(7) Fryer, R. M.; Muthukumarana, A.; Harrison, P. C.; Nodop Mazurek, S.; Chen, R. R.; Harrington, K. E.; Dinallo, R. M.; Horan, J. C.; Patnaude, L.; Modis, L. K.; Reinhart, G. A. The clinically-tested S1P receptor agonists, FTY720 and BAF312, demonstrate subtype-specific bradycardia ($S1P_1$) and hypertension ($S1P_3$) in rat. *PloS One* **2012**, *7*, e52985.

(8) Gergely, P.; Nuesslein-Hildesheim, B.; Guerini, D.; Brinkmann, V.; Traebert, M.; Bruns, C.; Pan, S.; Gray, N. S.; Hinterding, K.; Cooke, N. G.; Groenewegen, A.; Vitaliti, A.; Sing, T.; Luttringer, O.; Yang, J.; Gardin, A.; Wang, N.; Crumb, W. J., Jr.; Saltzman, M.; Rosenberg, M.; Wallstrom, E. The selective

sphingosine 1-phosphate receptor modulator BAF312 redirects lymphocyte distribution and has species-specific effects on heart rate. *Br. J. Pharmacol.* **2012**, *167*, 1035-1047.

(9) Murakami, A.; Takasugi, H.; Ohnuma, S.; Koide, Y.; Sakurai, A.; Takeda, S.; Hasegawa, T.; Sasamori, J.; Konno, T.; Hayashi, K.; Watanabe, Y.; Mori, K.; Sato, Y.; Takahashi, A.; Mochizuki, N.; Takakura, N. Sphingosine 1-phosphate (S1P) regulates vascular contraction via $S1P_3$ receptor: Investigation based on a new $S1P_3$ receptor antagonist. *Mol. Pharmacol.* **2010**, *77*, 704-713.

(10) Li, M. H.; Sanchez, T.; Pappalardo, A.; Lynch, K. R.; Hla, T.; Ferrer, F. Induction of antiproliferative connective tissue growth factor expression in Wilms' tumor cells by sphingosine-1-phosphate receptor 2. *Mol. Cancer Res.* **2008**, *6*, 1649-1656.

(11) Plano, D.; Amin, S.; Sharma, A. K. Importance of sphingosine kinase (SphK) as a target in developing cancer therapeutics and recent developments in the synthesis of novel SphK inhibitors. *J. Med. Chem.* **2014**, *57*, 5509-5524.

(12) Ishii, M.; Egen, J. G.; Klauschen, F.; Meier-Schellersheim, M.; Saeki, Y.; Vacher, J.; Proia, R. L.; Germain, R. N. Sphingosine-1-phosphate mobilizes osteoclast precursors and regulates bone homeostasis. *Nature* **2009**, *458*, 524-528.

(13) Cross, A. H.; Klein, R. S.; Piccio, L. Rituximab combination therapy in relapsing multiple sclerosis. *Ther. Adv. Neurol. Disord.* **2012**, *5*, 311-319.

(14) Dong, J.; Wang, H.; Wu, G.; Zhao, J.; Zhang, L.; Zuo, L.; Zhu, W.; Gong, J.; Li, Y.; Gu, L.; Li, J. Oral treatment with SEW2871, a sphingosine-1-phosphate type 1 receptor agonist, ameliorates experimental colitis in interleukin-10 gene deficient mice. *Clin. Exp. Immunol.* **2014**, *177*, 94-101.

(15) McCandless, E. E.; Budde, M.; Lees, J. R.; Dorsey, D.; Lyng, E.; Klein, R. S. IL-1R signaling within the central nervous system regulates CXCL12 expression at the blood-brain barrier and disease severity during experimental autoimmune encephalomyelitis. *J. Immunol.* **2009**, *183*, 613-620.

(16) Moberly, J. B.; Rohatagi, S.; Zahir, H.; Hsu, C.; Noveck, R. J.; Truitt, K. E. Pharmacological modulation of peripheral T and B lymphocytes by a selective sphingosine 1-phosphate receptor-1 modulator. *J. Clin. Pharmacol.* **2012**, *52*, 996-1006.

(17) Graler, M. H. Targeting sphingosine 1-phosphate (S1P) levels and S1P receptor functions for therapeutic immune interventions. *Cell. Physiol. Biochem.* **2010**, *26*, 79-86.

(18) Holman, D. W.; Klein, R. S.; Ransohoff, R. M. The blood-brain barrier, chemokines and multiple sclerosis. *Biochim. Biophys. Acta* **2011**, *1812*, 220-230.

(19) Ohno, T.; Hasegawa, C.; Nakade, S.; Kitagawa, J.; Honda, N.; Ogawa, M. The prediction of human response to ONO-4641, a sphingosine 1-phosphate receptor modulator, from preclinical data based on pharmacokinetic-pharmacodynamic modeling. *Biopharm. Drug Dispos.* **2010**, *31*, 396-406.

(20) McCandless, E. E.; Piccio, L.; Woerner, B. M.; Schmidt, R. E.; Rubin, J. B.; Cross, A. H.; Klein, R. S. Pathological expression of CXCL12 at the blood-brain barrier correlates with severity of multiple sclerosis. *Am. J. Pathol.* **2008**, *172*, 799-808.

(21) Wang, Z.; Sims, C. R.; Patil, N. K.; Gokden, N.; Mayeux, P. R. Pharmacologic targeting of sphingosine-1-phosphate receptor 1 improves the renal microcirculation during sepsis in the mouse. *J. Pharmacol. Exp. Ther.* **2015**, *352*, 61-66.

(22) Wong, D. F.; Tauscher, J.; Grunder, G. The role of imaging in proof of concept for CNS drug discovery and development. *Neuropsychopharmacology* **2009**, *34*, 187-203.

(23) Eckelman, W. C.; Kilbourn, M. R.; Mathis, C. A. Discussion of targeting proteins in vivo: in vitro guidelines. *Nucl. Med. Biol.* **2006**, *33*, 449-451.

(24) Eckelman, W. C.; Mathis, C. A. Targeting proteins in vivo: in vitro guidelines. *Nucl. Med. Biol.* **2006**, *33*, 161-164.

(25) Briard, E.; Orain, D.; Beerli, C.; Billich, A.; Streiff, M.; Bigaud, M.; Auberson, Y. P. BZM055, an iodinated radiotracer candidate for PET and SPECT imaging of myelin and FTY720 brain distribution. *ChemMedChem* **2011**, *6*, 667-677.

(26) Prasad, V. P.; Wagner, S.; Keul, P.; Hermann, S.; Levkau, B.; Schäfers, M.; Haufe, G. Synthesis of fluorinated analogues of sphingosine-1-phosphate antagonists as potential radiotracers for molecular imaging using positron emission tomography. *Bioorg. Med. Chem.* **2014**, *22*, 5168-5181.

(27) Shaikh, R. S.; Schilson, S. S.; Wagner, S.; Hermann, S.; Keul, P.; Levkau, B.; Schafers, M.; Haufe, G. Synthesis and evaluation of fluorinated fingolimod (FTY720) analogues for sphingosine-1-phosphate receptor molecular imaging by positron emission tomography. *J. Med. Chem.* **2015**, *58*, 3471-3484.

(28) Yue, X.; Jin, H.; Liu, H.; Rosenberg, A. J.; Klein, R. S.; Tu, Z. A potent and selective C-11 labeled PET tracer for imaging sphingosine-1-phosphate receptor 2 in the CNS demonstrates sexually dimorphic expression. *Org. Biomol. Chem.* **2015**, *13*, 7928-7939.

(29) Jin, H.; Yang, H.; Liu, H.; Zhang, Y.; Zhang, X.; Rosenberg, A. J.; Liu, Y.; Lapi, S. E.; Tu, Z. A promising carbon-11-labeled sphingosine-1-phosphate receptor 1-specific PET tracer for imaging vascular injury. *J. Nucl. Cardiol.* [Online early access]. DOI:10.1007/s12350-015-0391-1. Published Online: February 02, 2016.

(30) Liu, H.; Jin, H.; Yue, X.; Luo, Z.; Liu, C.; Rosenberg, A. J.; Tu, Z. PET imaging study of S1PR1 expression in a rat model of multiple sclerosis. *Mol. Imaging Biol.* [Online early access]. DOI: 10.1007/s11307-016-0944-y. Published Online: March 14, 2016.

(31) Deng, G.; Meng, Q.; Liu, Q.; Xu, X.; Xu, Q.; Ren, F.; Guo, T. B.; Lu, H.; Xiang, J. N.; Elliott, J. D.; Lin, X. Identification of benzoxazole analogs as novel, $S1P_3$ sparing $S1P_1$ agonists. *Bioorg. Med. Chem. Lett.* **2012**, *22*, 3973-3977.

(32) Quattropani, A.; Sauer, W. H.; Crosignani, S.; Dorbais, J.; Gerber, P.; Gonzalez, J.; Marin, D.; Muzerelle, M.; Beltran, F.; Nichols, A.; Georgi, K.; Schneider, M.; Vitte, P. A.; Eligert, V.; Novo-Perez, L.; Hantson, J.; Nock, S.; Carboni, S.; de Souza, A. L.; Arrighi, J. F.; Boschert, U.; Bombrun, A. Pharmacophore-based design of novel oxadiazoles as selective sphingosine-1-phosphate (S1P) receptor agonists with in vivo efficacy. *ChemMedChem* **2015**, *10*, 688-714.

(33) Li, Z.; Chen, W.; Hale, J. J.; Lynch, C. L.; Mills, S. G.; Hajdu, R.; Keohane, C. A.; Rosenbach, M. J.; Milligan, J. A.; Shei, G. J.; Chrebet, G.; Parent, S. A.; Bergstrom, J.; Card, D.; Forrest, M.; Quackenbush, E. J.; Wickham, L. A.; Vargas, H.; Evans, R. M.; Rosen, H.; Mandala, S. Discovery of potent 3,5-diphenyl-1,2,4-oxadiazole sphingosine-1-phosphate-1 ($S1P_1$) receptor agonists with exceptional selectivity against $S1P_2$ and $S1P_3$. *J. Med. Chem.* **2005**, *48*, 6169-6173.

(34) Rosenberg, A. J.; Liu, H.; Tu, Z. A practical process for the preparation of [^{32}P]S1P and binding assay for S1P receptor ligands. *Appl. Radiat. Isot.* **2015**, *102*, 5-9.

(35) Sanna, M. G.; Liao, J.; Jo, E.; Alfonso, C.; Ahn, M. Y.; Peterson, M. S.; Webb, B.; Lefebvre, S.; Chun, J.; Gray, N.; Rosen, H. Sphingosine 1-phosphate (S1P) receptor subtypes $S1P_1$ and $S1P_3$, respectively, regulate lymphocyte recirculation and heart rate. *J. Biol. Chem.* **2004**, *279*, 13839-13848.

(36) Chen, D. L.; Zhou, D.; Chu, W.; Herrbrich, P.; Engle, J. T.; Griffin, E.; Jones, L. A.; Rothfuss, J. M.; Geraci, M.; Hotchkiss, R. S.; Mach, R. H. Radiolabeled isatin binding to caspase-3 activation induced by anti-Fas antibody. *Nucl. Med. Biol.* **2012**, *39*, 137-144.

(37) Sic, H.; Kraus, H.; Madl, J.; Flittner, K. A.; von Munchow, A. L.; Pieper, K.; Rizzi, M.; Kienzler, A. K.; Ayata, K.; Rauer, S.; Kleuser, B.; Salzer, U.; Burger, M.; Zirlik, K.; Lougaris, V.; Plebani, A.; Romer, W.; Loeffler, C.; Scaramuzza, S.; Villa, A.; Noguchi, E.; Grimbacher, B.; Eibel, H. Sphingosine-1-phosphate receptors control B-cell migration through signaling components associated with primary immunodeficiencies, chronic lymphocytic leukemia, and multiple sclerosis. *J. Allergy Clin. Immunol.* **2014**, *134*, 420-428.

(38) Cavone, L.; Felici, R.; Lapucci, A.; Buonvicino, D.; Pratesi, S.; Muzzi, M.; Hakiki, B.; Maggi, L.; Peruzzi, B.; Caporale, R.; Annunziato, F.; Amato, M. P.; Chiarugi, A. Dysregulation of sphingosine 1 phosphate receptor-1 (S1P1) signaling and regulatory lymphocyte-dependent immunosuppression in a model of post-fingolimod MS rebound. *Brain, Behav., Immun.* **2015**, *50*, 78-86.

(39) Poulain, R. F.; Tartar, A. L.; Déprez, B. t. P. Parallel synthesis of 1,2,4-oxadiazoles from carboxylic acids using an improved, uronium-based, activation. *Tetrahedron Lett.* **2001**, *42*, 1495-1498.

(40) Waterhouse, R. N. Determination of lipophilicity and its use as a predictor of blood-brain barrier penetration of molecular imaging agents. *Mol. Imaging Biol.* **2003**, *5*, 376-389.

(41) Komiya, T.; Sato, K.; Shioya, H.; Inagaki, Y.; Hagiya, H.; Kozaki, R.; Imai, M.; Takada, Y.; Maeda, T.; Kurata, H.; Kurono, M.; Suzuki, R.; Otsuki, K.; Habashita, H.; Nakade, S. Efficacy and immunomodulatory actions of ONO-4641, a novel selective agonist for sphingosine 1-phosphate receptors 1 and 5, in preclinical models of multiple sclerosis. *Clin. Exp. Immunol.* **2013**, *171*, 54-62.

(42) Gibson, R. E. *In vitro* approaches to site-specific imaging agents. In *Targeted Molecular Imaging*, Welch, M. J., Eckelman, W. C., Eds.; CRC Press, Taylor & Francis Group: Boca Raton, FL, 2012; pp 3-15.

(43) Hanson, M. A.; Roth, C. B.; Jo, E.; Griffith, M. T.; Scott, F. L.; Reinhart, G.; Desale, H.; Clemons, B.; Cahalan, S. M.; Schuerer, S. C.; Sanna, M. G.; Han, G. W.; Kuhn, P.; Rosen, H.; Stevens, R. C. Crystal structure of a lipid G protein-coupled receptor. *Science* **2012**, *335*, 851-855.

(44) Peng, X.; Hassoun, P. M.; Sammani, S.; McVerry, B. J.; Burne, M. J.; Rabb, H.; Pearse, D.; Tuder, R. M.; Garcia, J. G. Protective effects of sphingosine 1-phosphate in murine endotoxin-induced inflammatory lung injury. *Am. J. Respir. Crit. Care Med.* **2004**, *169*, 1245-1251.

(45) Kono, M.; Tucker, A. E.; Tran, J.; Bergner, J. B.; Turner, E. M.; Proia, R. L. Sphingosine-1-phosphate receptor 1 reporter mice reveal receptor activation sites in vivo. *J. Clin. Invest.* **2014**, *124*, 2076-2086.

(46) Gonzalez-Cabrera, P. J.; Jo, E.; Sanna, M. G.; Brown, S.; Leaf, N.; Marsolais, D.; Schaeffer, M. T.; Chapman, J.; Cameron, M.; Guerrero, M.; Roberts, E.; Rosen, H. Full pharmacological efficacy of a novel $S1P_1$ agonist that does not require S1P-like headgroup interactions. *Mol. Pharmacol.* **2008**, *74*, 1308-1318.

(47) Tomlinson, R. E.; Silva, M. J.; Shoghi, K. I. Quantification of skeletal blood flow and fluoride metabolism in rats using PET in a pre-clinical stress fracture model. *Mol. Imaging Biol.* **2012**, *14*, 348-354.

(48) Shiomi, S.; Iwata, Y.; Sasaki, N.; Morikawa, H.; Tamori, A.; Habu, D.; Takeda, T.; Nishiguchi, S.; Kuroki, T.; Ochi, H. Assessment of hepatic blood flow by PET with ^{15}O water: Correlation between per-rectal portal scintigraphy with $^{99}Tc^m$-pertechnetate and scintigraphy with $^{99}Tc^m$-GSA. *Nucl. Med. Commun.* **2000**, *21*, 533-538.

(49) Ghibellini, G.; Leslie, E. M.; Pollack, G. M.; Brouwer, K. L. Use of Tc-99m mebrofenin as a clinical probe to assess altered hepatobiliary transport: Integration of in vitro, pharmacokinetic modeling, and simulation studies. *Pharm. Res.* **2008**, *25*, 1851-1860.

(50) Joseph, B.; Bhargava, K. K.; Tronco, G. G.; Palestro, C. J.; Gupta, S. Systemic and local release of inflammatory cytokines regulates hepatobiliary excretion of ^{99m}Tc-mebrofenin. *Nucl. Med. Commun.* **2008**, *29*, 336-344.

(51) Schurer, S. C.; Brown, S. J.; Gonzalez-Cabrera, P. J.; Schaeffer, M. T.; Chapman, J.; Jo, E.; Chase, P.; Spicer, T.; Hodder, P.; Rosen, H. Ligand-binding pocket shape differences between sphingosine 1-phosphate (S1P) receptors $S1P_1$ and $S1P_3$ determine efficiency of chemical probe identification by ultrahigh-throughput screening. *ACS Chem. Biol.* **2008**, *3*, 486-498.

(52) Brenner, C.; Galluzzi, L.; Kepp, O.; Kroemer, G. Decoding cell death signals in liver inflammation. *J. Hepatol.* **2013**, *59*, 583-594.

(53) Schroder, M.; Richter, C.; Juan, M. H.; Maltusch, K.; Giegold, O.; Quintini, G.; Pfeilschifter, J. M.; Huwiler, A.; Radeke, H. H. The sphingosine kinase 1 and S1P1 axis specifically counteracts LPS-induced IL-12p70 production in immune cells of the spleen. *Mol. Immunol.* **2011**, *48*, 1139-1148.

(54) Zhou, D.; Lee, H.; Rothfuss, J. M.; Chen, D. L.; Ponde, D. E.; Welch, M. J.; Mach, R. H. Design and synthesis of 2-amino-4-methylpyridine analogues as inhibitors for inducible nitric oxide synthase and in vivo evaluation of [^{18}F]6-(2-fluoropropyl)-4-methyl-pyridin-2-amine as a potential PET tracer for inducible nitric oxide synthase. *J. Med. Chem.* **2009**, *52*, 2443-2453.

Table 1

Table 1. Structure activity relationships in the benzoxazole core series

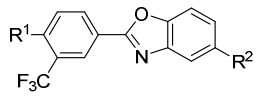

Compound	R^1	R^2	$S1P_1$ IC_{50} (nM)	$S1P_1$ EC_{50} (nM)	$cLogD_{7.4}$
15a	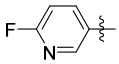	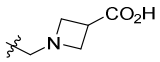	**92.7 ± 35.3**	**-**	**2.08**
15b		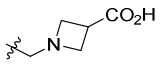	**76.4 ± 21.6**	**-**	**2.21**
16	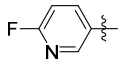	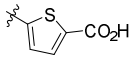	**334 ± 59**	**2.99**	**4.10**
18a	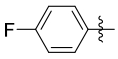	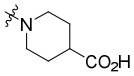	**486 ± 69**	**0.76**	**3.72**
18b	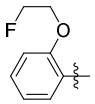	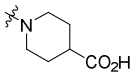	**894 ± 367**	**3.04**	**3.69**
18c	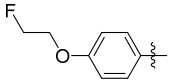	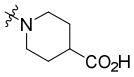	**114 ± 73**	**11.1**	**3.84**
18d	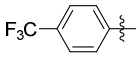	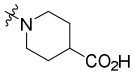	**498 ± 335**	**4.47**	**4.76**
18e	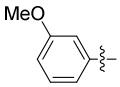	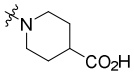	**95.7 ± 25.1**	**4.90**	**3.56**

Table 2

Table 2. Structure activity relationships in the oxadiazole core series

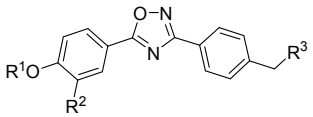

Compound	R^1	R^2	Head Group (R^3)	IC_{50} (nM)			$cLogD_{7.4}$
				$S1P_1$	$S1P_2$	$S1P_3$	
28a	Et	H	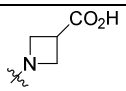	8.53 ± 3.14	> 1000	> 1000	1.10
28b	FCH_2CH_2	H	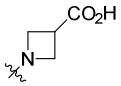	9.94 ± 1.03	> 1000	> 1000	0.80
28c	FCH_2CH_2	CF_3	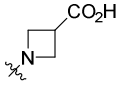	2.63 ± 0.27	> 1000	> 1000	2.32
28d	FCH_2CH_2	CF_3	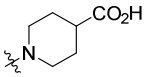	45.4 ± 2.7	> 1000	> 1000	3.02
28e	FCH_2CH_2	CF_3	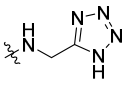	509 ± 167	-	-	2.08
28f	Me	CF_3	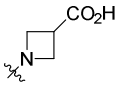	103 ± 21	-	-	2.09
26c	FCH_2CH_2	CF_3		6.67 ± 0.70	> 1000	> 1000	4.88

Table 3

Table 3. Biodistribution of [^{18}F]28c in Adult Male SD Rats (%ID/g ± SD)(n=4)

Organ	5 min	30 min	60 min	120 min
Blood	0.304 ± 0.058	0.240 ± 0.024	0.223 ± 0.007	0.178 ± 0.039
Lung	0.753 ± 0.097	0.413 ± 0.005	0.341 ± 0.024	0.272 ± 0.053
Liver	6.076 ± 1.134	5.509 ± 0.567	5.081 ± 0.324	3.355 ± 0.772
Spleen	0.589 ± 0.067	0.282 ± 0.030	0.251 ± 0.014	0.202 ± 0.033
Kidney	2.026 ± 0.250	1.080 ± 0.000	1.117 ± 0.052	0.845 ± 0.091
Muscle	0.121 ± 0.013	0.145 ± 0.013	0.156 ± 0.010	0.135 ± 0.007
Fat	0.051 ± 0.011	0.061 ± 0.003	0.051 ± 0.003	0.059 ± 0.011
Heart	0.811 ± 0.167	0.445 ± 0.030	0.379 ± 0.015	0.316 ± 0.061
Brain	0.027 ± 0.004	0.018 ± 0.002	0.017 ± 0.002	0.015 ± 0.002
Bone	0.215 ± 0.027	0.114 ± 0.002	0.105 ± 0.100	0.100 ± 0.012
Pancreas	0.755 ± 0.207	0.320 ± 0.047	0.298 ± 0.089	0.265 ± 0.128
Thymus	0.150 ± 0.023	0.151 ± 0.010	0.161 ± 0.007	0.182 ± 0.013

Scheme 1

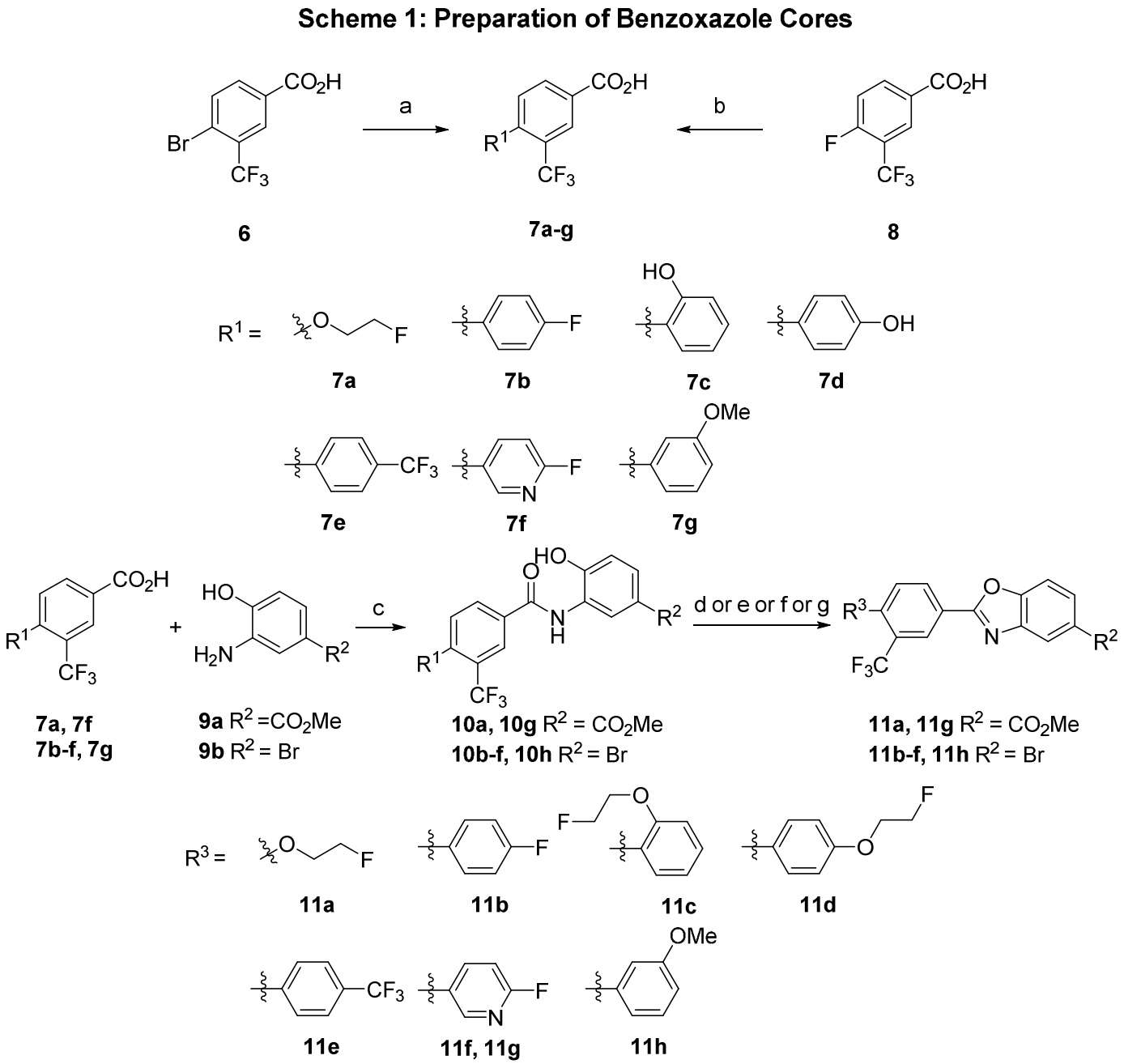

Reagents and Conditions: (a) $Pd(OAc)_2$, SPhos, CsF, $R^1B(OH)_2$, 1,4-dioxane/H_2O for **7b-g**; (b) NaH, R^1OH, DMSO for **7a**; (c) (i)$(COCl)_2$, cat. DMF, CH_2Cl_2; (ii) Et_3N, DMAP, CH_2Cl_2; (d) *p*-TsOH, toluene for **11a, 11b, 11e, 11h;** (e) (i) *p*-TsOH, toluene; (ii) Cs_2CO_3, fluoroethyltosylate, DMF for **11c, 11d**; (f) Ph_3P, DIAD, THF for **11f**; (g) PPTS, toluene for **11g**.

Scheme 2

Scheme 2: Synthesis of Benzoxazole Targets

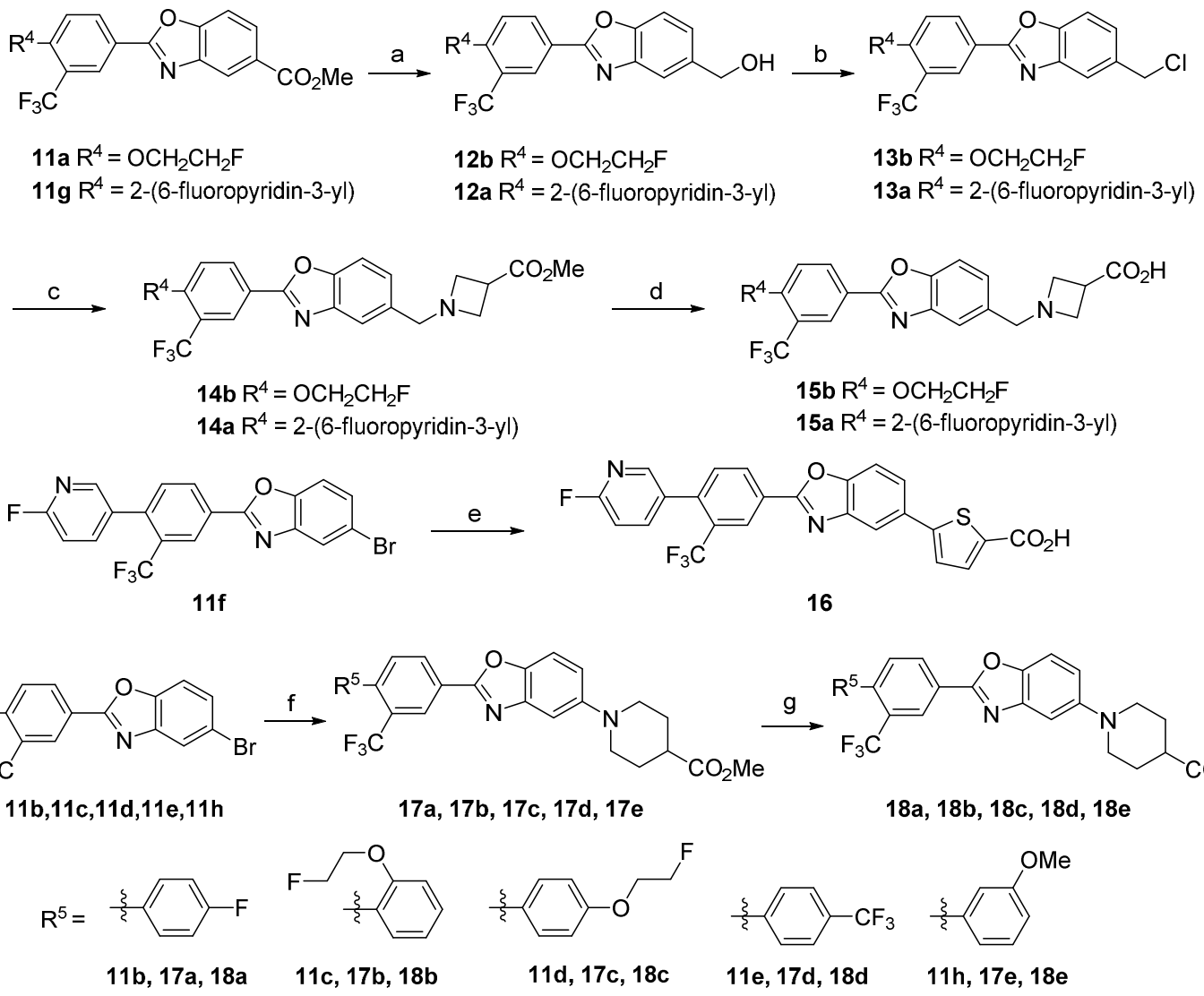

Reagents and Conditions: (a) DIBAl-H, THF; (b) cyanuric chloride, DMF, CH_2Cl_2; (c) methyl azetidine-3-carboxylate hydrochloride, *i*-Pr_2NEt, MeCN; (d) LiOH, THF/H_2O; (e) $Pd(OAc)_2$, SPhos, KF, 2-carboxythiophene-5-boronic acid, 1,4-Dioxane/H_2O; (f) $Pd_2(dba)_3$•$CHCl_3$, XPhos, NaO^tBu, methyl piperidine-4-carboxylate; (g) LiOH, THF/H_2O.

Scheme 3

Scheme 3: Synthesis of Benzoxazole Targets

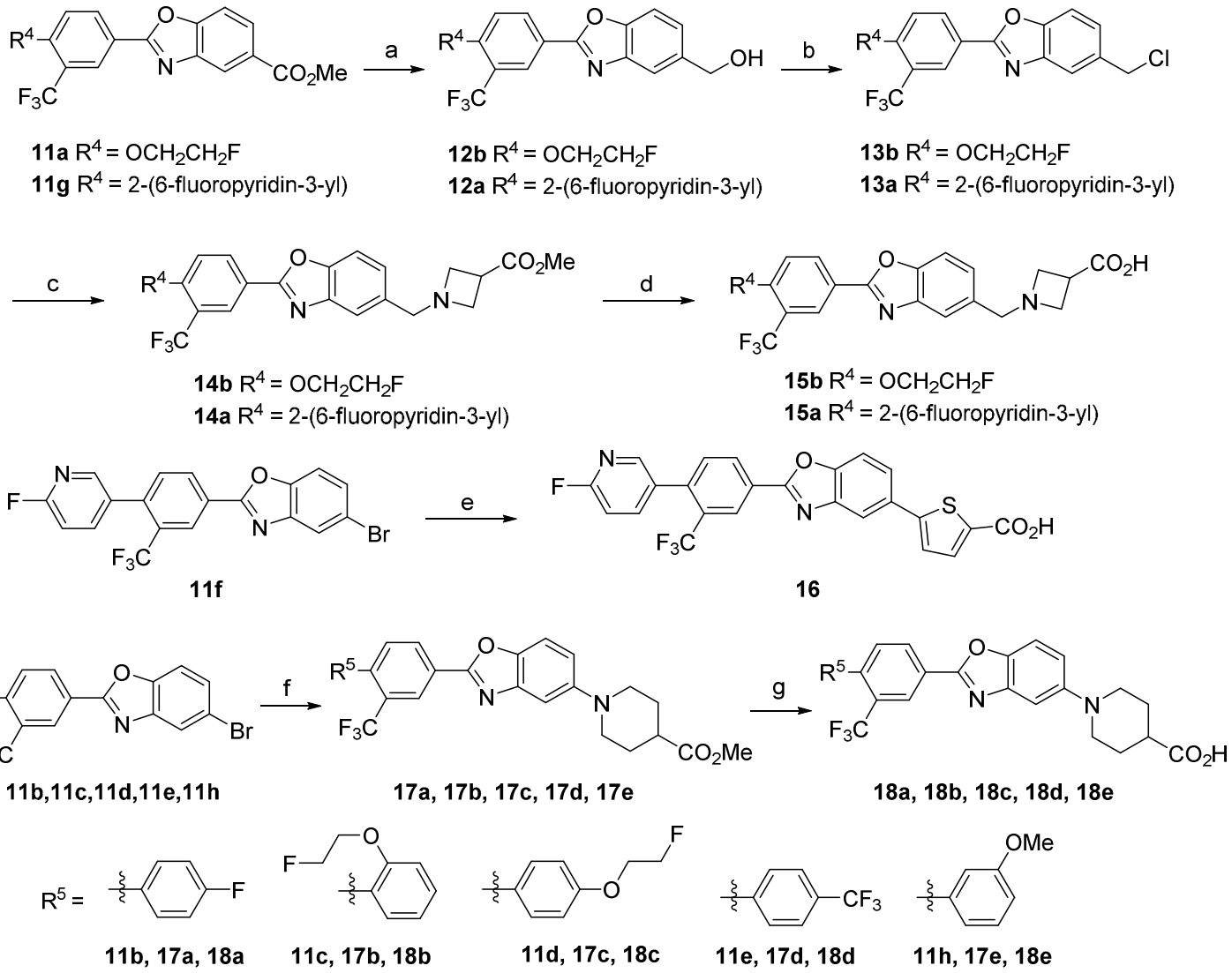

Reagents and Conditions: (a) DIBAl-H, THF; (b) cyanuric chloride, DMF, CH_2Cl_2; (c) methyl azetidine-3-carboxylate hydrochloride, *i*-Pr_2NEt, MeCN; (d) LiOH, THF/H_2O; (e) $Pd(OAc)_2$, SPhos, KF, 2-carboxythiophene-5-boronic acid, 1,4-Dioxane/H_2O; (f) $Pd_2(dba)_3$•$CHCl_3$, XPhos, NaO^{t}Bu, methyl piperidine-4-carboxylate; (g) LiOH, THF/H_2O.

Scheme 4

Scheme 4: Synthesis of Radiolabeling Precursor 32

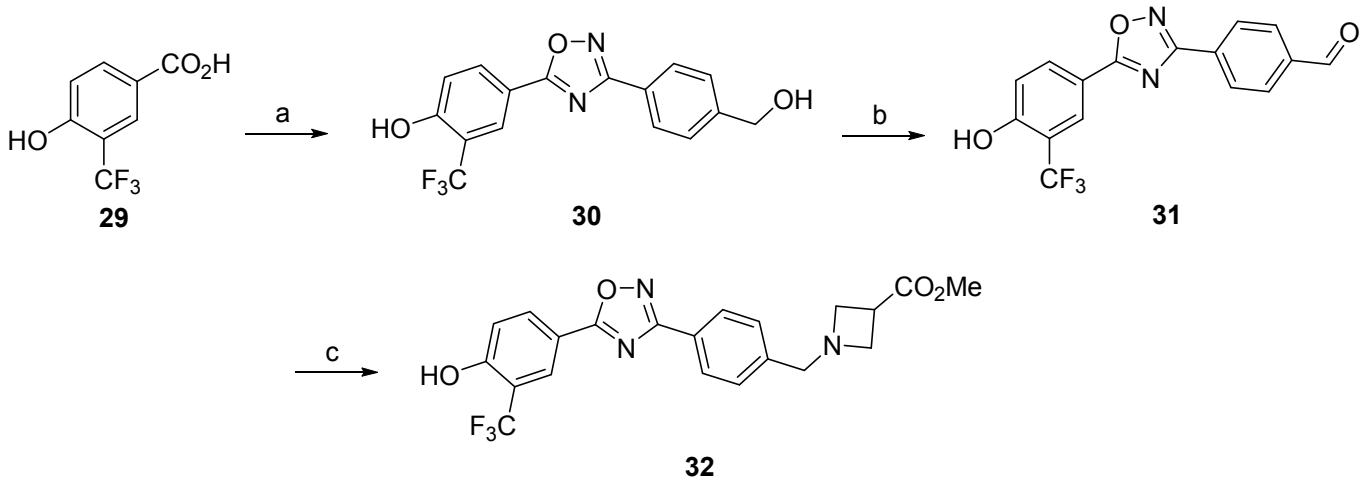

Reagents and Conditions: (a) TBTU, HOBt, **25**, DMF; (b) MnO_2, 1,4-Dioxane (c) methyl azetidine-3-carboxylate HCl, $NaBH_3CN$, AcOH, DIPEA, MeOH.

Scheme 5

Scheme 5: Preparation of Direct Radiolabeling Precursor 34

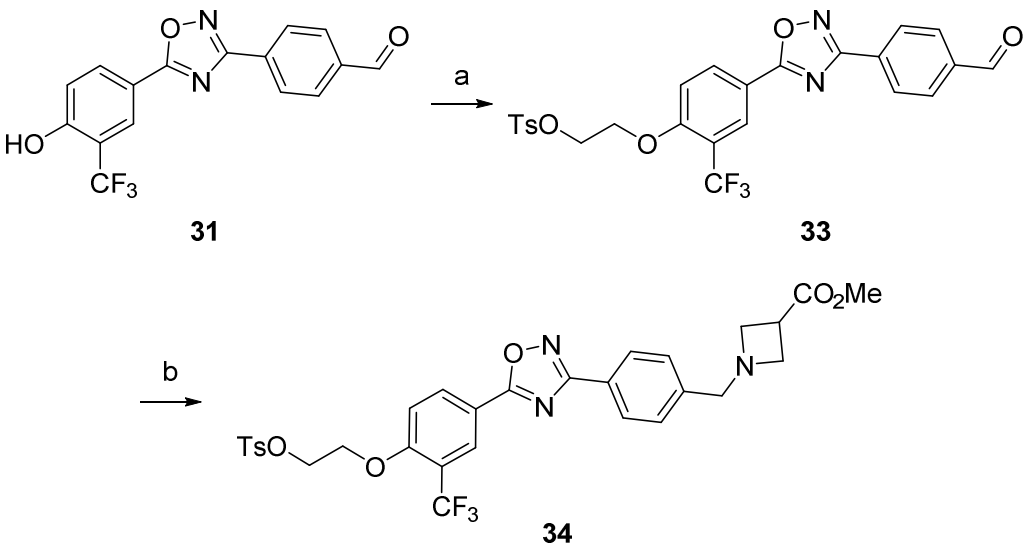

Reagents and Conditions: (a) $(CH_2OTs)_2$, K_2CO_3, MeCN; (b) (i) DIPEA, 1,2-DCE/MeOH; (ii) $NaBH(OAc)_3$, AcOH, 1,2-DCE.

Scheme 6

Scheme 6: Radiosynthesis of [^{18}F]28c

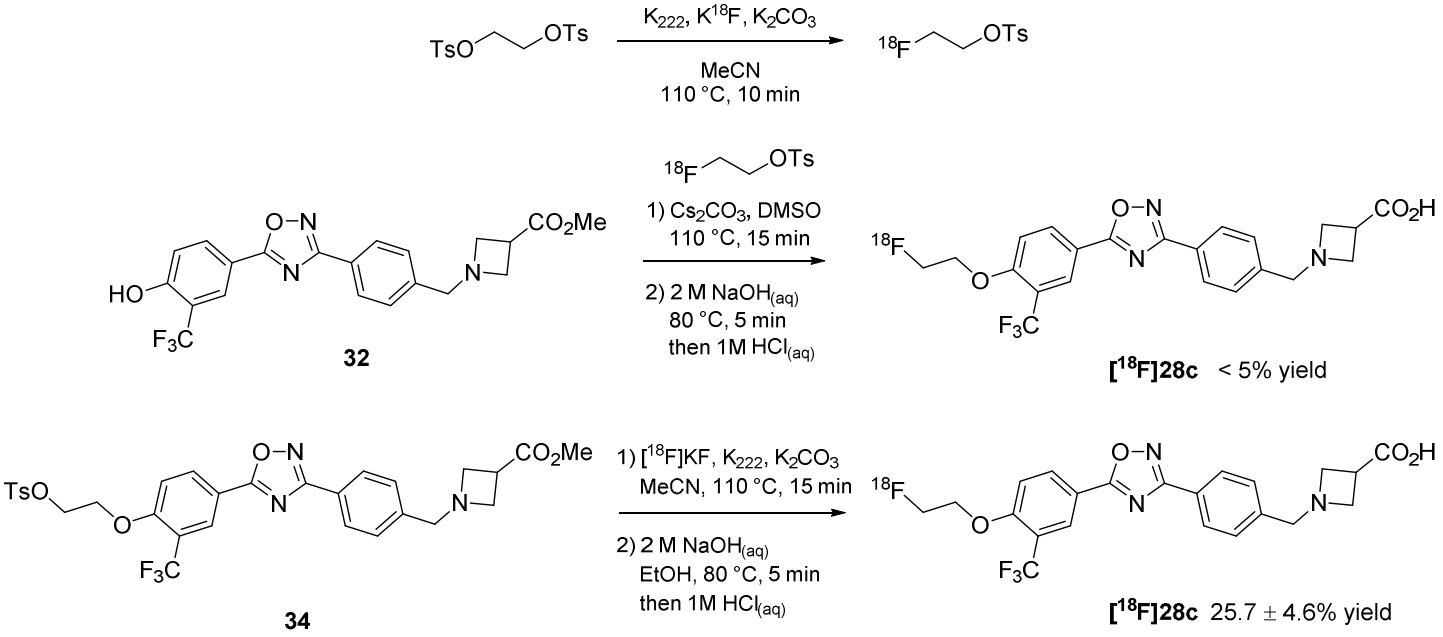

Figure 1

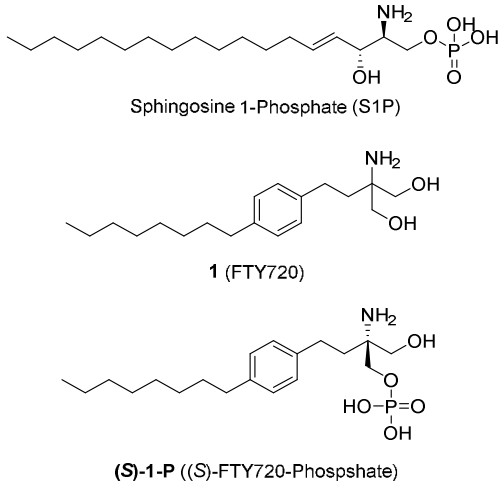

Figure 1. Structures of S1P, FTY720 and (*S*)-FTY720-Phosphate

Figure 2

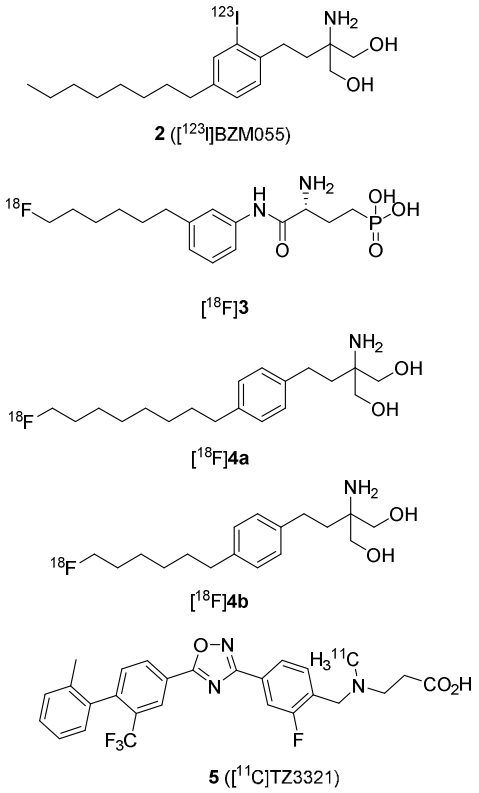

Figure 2. Structures of S1P receptor imaging agents

Figure 3

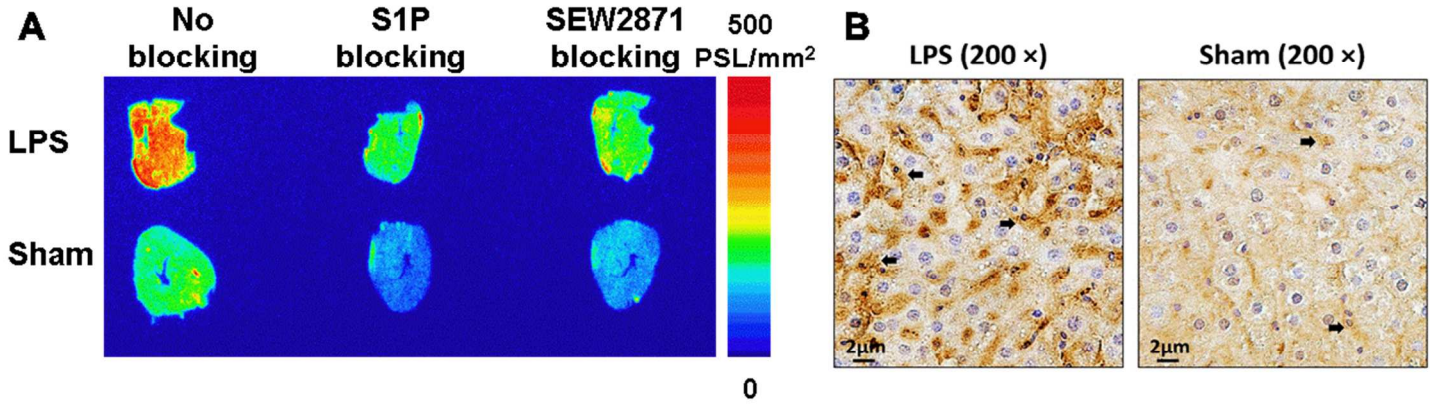

Figure 3. (A)Representative *in vitro* autoradiographic images of serial liver sections from LPS-treated and sham mice after incubation with [^{18}F]28c under baseline or blocking conditions. (B) IHC staining for $S1P_1$ in mouse liver sections. Positive staining for $S1P_1$ (brown, indicated by black arrows) was observed in the liver of both LPS-treated (left) and sham (right) mice. The number of $S1P_1$-positive cells in the liver of LPS-treated mice was much greater than in sham mice.

Figure 4

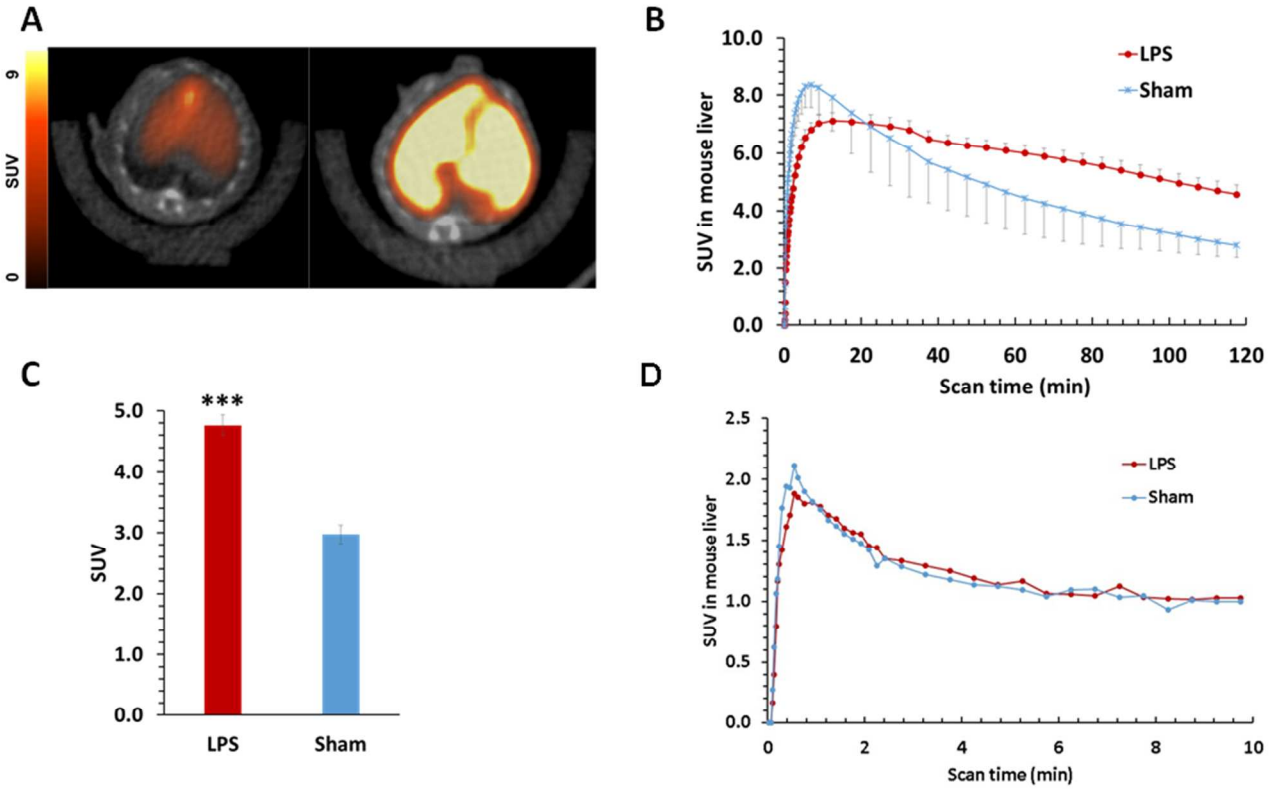

Figure 4. (A) Representative summed 120 min transverse PET/CT images of [^{18}F]**28c** in a sham (left) and LPS-treated (right) mouse. (B) Liver time-activity curves (TAC) of [^{18}F]**28c** standardized uptake values (SUV) in sham and LPS-treated mice. (C) Sham vs. LPS-treated summed liver SUVs from 100-120 min post-injection. $P < 0.001$. (D) Liver TACs of [^{15}O]H_2O in sham and LPS-treated mice.

Figure 5

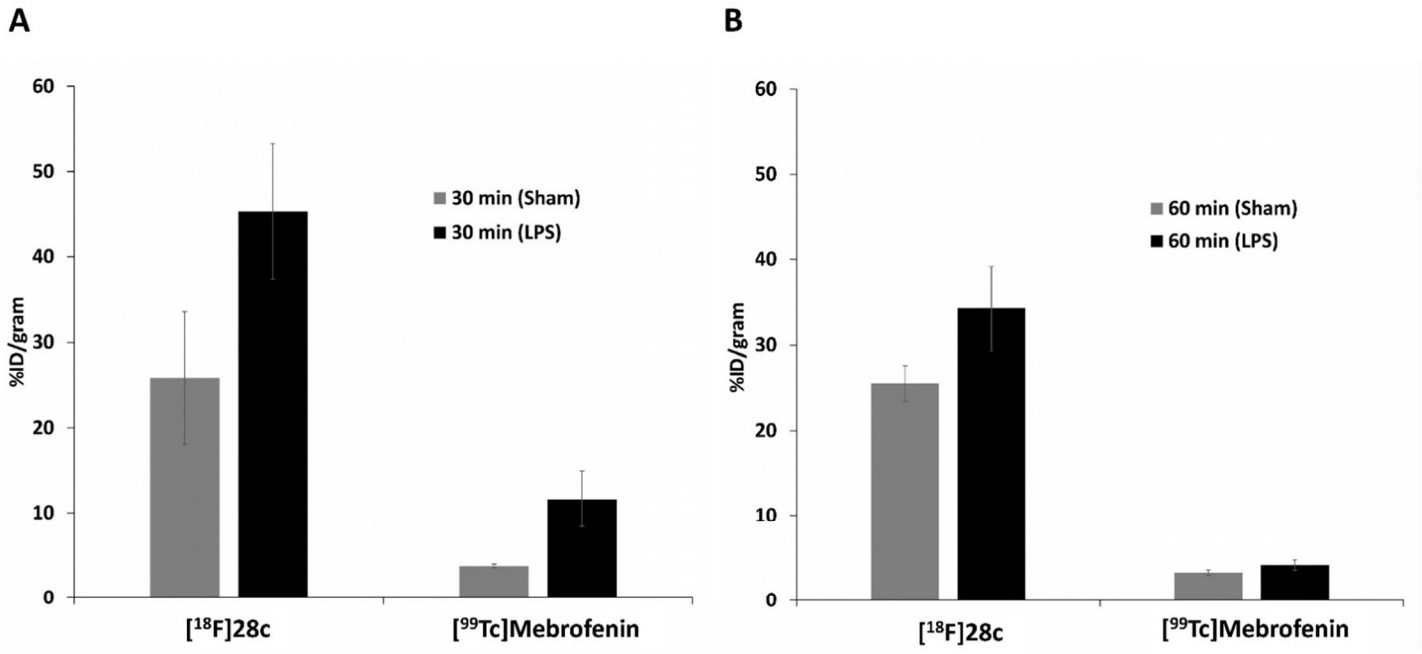

Figure 5 Liver uptake in LPS-treated and sham mice 30 min (A) and 60 min (B) post-injection of [^{18}F]**28c** or [^{99m}Tc]mebrofenin

Table of Contents Graphic

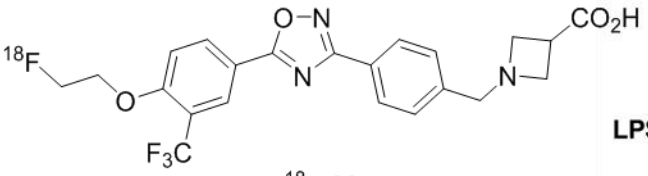

[^{18}F]**28c**

S1P$_1$ IC_{50} = 2.63 ± 0.27 nM
S1P$_2$ IC_{50} > 1000 nM
S1P$_3$ IC_{50} > 1000 nM